Length scales and types of heterogeneities along the deep subduction interface: Insights from exhumed rocks on Syros Island, Greece

Author(s):
Kotowski, Alissa J.; Behr, Whitney M.

Publication date:
2019-08-01

Permanent link:
https://doi.org/10.3929/ethz-b-000358300

Originally published in:
Geosphere 15(4), https://doi.org/10.1130/GES02037.1

Research Paper

THEMED ISSUE: Subduction Top to Bottom 2

GEOSPHERE

GEOSPHERE, v. 15, no. 4

https://doi.org/10.1130/GES02037.1

15 figures; 1 set of supplemental files

CORRESPONDENCE: kotowski@utexas.edu

CITATION: Kotowski, A.J., and Behr, W.M., 2019, Length scales and types of heterogeneities along the deep subduction interface: Insights from exhumed rocks on Syros Island, Greece: Geosphere, v. 15, no. 4, p. 1038–1065, https://doi.org/10.1130/GES02037.1.

Science Editor: Shanaka de Silva
Guest Associate Editor: Gray Bebout

Received 14 July 2018
Revision received 15 March 2019
Accepted 15 May 2019

Published online 24 June 2019

Length scales and types of heterogeneities along the deep subduction interface: Insights from exhumed rocks on Syros Island, Greece

Alissa J. Kotowski[1] and Whitney M. Behr[1,*]

[1]Department of Geological Sciences, Jackson School of Geosciences, University of Texas at Austin, 2275 Speedway Stop C9000, Austin, Texas 78712-1722, USA

ABSTRACT

We use structural and microstructural observations from exhumed subduction-related rocks exposed on Syros Island (Cyclades, Greece) to provide constraints on the length scales and types of heterogeneities that occupy the deep subduction interface, with possible implications for episodic tremor and slow slip. We selected three Syros localities that represent different oceanic protoliths and deformation conditions within a subduction interface shear zone, including: (1) prograde subduction of oceanic crust to eclogite facies; (2) exhumation of oceanic crust from eclogite through blueschist-greenschist facies; and (3) exhumation of mixed mafic crust and sediments from eclogite through blueschist-greenschist facies. All three localities preserve rheological heterogeneities that reflect metamorphism of primary lithological, geochemical, and/or textural variations in the subducted protoliths and that take the form of brittle pods and lenses within a viscous matrix. Microstructural observations indicate that the matrix lithologies (blueschists and quartz-rich metasediments) deformed by distributed power-law viscous flow accommodated by dislocation creep in multiple mineral phases. We estimate bulk shear zone viscosities ranging from ~10^{18} to 10^{20} Pa-s, depending on the relative proportion of sediments to (partially eclogitized) oceanic crust. Eclogite and coarse-grained blueschist heterogeneities within the matrix preserve multiple generations of dilational shear fractures and veins formed under high-pressure conditions. The veins commonly show coeval or overprinting viscous shear, suggesting repeated cycles of frictional and viscous strain. These geologic observations are consistent with a mechanical model of episodic tremor and slow slip (ETS), in which the deep subduction interface is a rheologically heterogeneous distributed shear zone comprising transiently brittle (potentially tremor-genic) sub-patches within a larger, viscously creeping interface patch. Based on our observations of outcrop and map areas of heterogeneous patches and the sizes, distributions, and amounts of brittle offset recorded by heterogeneities, we estimate that simultaneous brittle failure of heterogeneities could produce tremor bursts with equivalent seismic moments of 4.5 × 10^{9}–4.7 × 10^{14} N m, consistent with seismic moments estimated from geophysical data at active subduction zones.

*Now at Geological Institute, Department of Earth Sciences, Swiss Federal Institute of Technology (ETH), 8092 Zurich, Switzerland

1. INTRODUCTION

The subduction interface is characterized by progressive downdip changes in metamorphic conditions, rheological properties, and fluid sources and pathways. Geodetic and seismological observations in modern subduction zones suggest that these downdip changes can be accompanied by important differences in seismic style. For example, shallow slow slip—an aseismic phenomenon characterized by transient, accelerated interface strain rates—has been observed up-dip of the seismogenic zone in several modern subduction zones, including Hikurangi (Douglas et al., 2005; Wallace and Beavan, 2010; Wallace et al., 2012), Northern Japan (Ito et al., 2013), Costa Rica (Dixon et al., 2014), and Nankai (Ito and Obara, 2006). This zone of shallow slow slip transitions downdip into a locked region that has the potential to release elastic strain in large, destructive earthquakes (e.g., Kanamori, 1986; Oleskevich et al., 1999). Below the locked megathrust zone, the behavior of the deep interface is especially complex. A growing body of land-based geodetic and microseismic observations suggests that deep interface deformation is characterized by transient accelerated aseismic slow slip events (SSEs) and low-frequency earthquakes (LFEs), together forming what is known as deep episodic tremor and slow slip (ETS) (e.g., Obara, 2002; Rogers and Dragert, 2003; Ito and Obara, 2006; Shelly et al., 2006; Beroza and Ide, 2011). LFEs and corresponding tremor bursts occur during and between SSEs throughout an ETS event (Ito et al., 2007; Shelly et al., 2007b). ETS events are capable of dissipating ~75% to nearly 100% of convergence-related stress downdip of ~25 km accumulated over years to decades (Chapman and Melbourne, 2009; Wallace and Beavan, 2010); of this fraction, seismic tremor accounts for 0.1% to ~20% of the total change in strain energy (Kao et al., 2010; Sweet et al., 2014). Understanding ETS events is crucial, as these events may load the megathrust up-dip and/or along strike, thereby increasing the potential for great subduction earthquakes (Dragert et al., 2004; Chapman and Melbourne, 2009; Segall and Bradley, 2012).

Each distinct zone of seismic behavior must be linked to deformation conditions, mechanisms, and types of heterogeneities within that region of the interface. For the shallow interface, these linkages can be detected through drilling (e.g., Moore, 1995), seismic imaging (Byrne et al., 1988; Abers, 1992), and continuous monitoring of seafloor deformation (e.g., Wallace et al., 2016).

Combined with numerical modeling and deformation experiments, these observations suggest that shallow slow slip events occur in regions of transitional frictional properties, under low effective stress and high pore fluid pressures (e.g., McCaffrey et al., 2008; Saffer and Wallace, 2015; Wallace et al., 2016). Some studies, for example, suggest that changes from velocity strengthening to velocity weakening along a planar frictional fault surface may explain unconventional, slow seismicity (Shibazaki and Shimamoto, 2007; Rubin, 2008), while others invoke protolith-induced rigidity contrasts within macroscopically ductile interface shear zones (Fagereng and Sibson, 2010; Saffer and Wallace, 2015; Fagereng and Den Hartog, 2016). Downdip within the locked zone, the spatial extents and distributions of megathrust earthquakes can also be linked with primary structural heterogeneities such as oceanic seamounts or other topographic highs, sediment subduction and corresponding changes in deformation mechanisms, and/or heterogeneous material and mechanical properties generated at the seismogenic front during compaction and dehydration (Cloos, 1992; Moore and Saffer, 2001; Husen et al., 2002; Gulick et al., 2011; Hicks et al., 2012).

The role of primary or generated heterogeneities in contributing to seismic behavior below the megathrust locked zone is less well understood, partly because direct observations of the plate interface are not possible at these depths (e.g., ≥25 km). This is also the depth range where pressure and temperature conditions begin to favor viscous creep mechanisms in most crustal minerals, depending on fluid pressure conditions and strain rates. A transition to viscous creep along the deep interface has the potential to "smear" and/or completely homogenize heterogeneities that may have once acted as frictional asperities at shallower depths, through ductile deformation and widening of the interface shear zone. By analogy with continental shear zones, amphibolite- and granulite-facies shear zones often show such homogenization, exemplified by penetrative, continuous shear of a wide range of protolith rock types (e.g., Fountain and Salisbury, 1981; Kenkmann and Dresen, 2002; Norris and Cooper, 2003). The discovery of ETS at high-pressure conditions in subduction zones, however, suggests that rheological heterogeneities still persist in a form that may affect seismic behavior. But what kinds of heterogeneities occupy the deep subduction interface? What are their rheological properties, length scales, and spatial distributions? And how do they relate to the heterogeneities that existed in protoliths prior to subduction? In this paper, we address these questions using eclogite-, blueschist-, and greenschist-facies rocks exposed on Syros Island, Greece. Syros is interpreted as a fossilized subduction shear zone recording deformation in several rock types over a wide range of pressure-temperature conditions and therefore may shed light on processes controlling transient phenomena such as ETS.

2. GEOLOGIC SETTING

Since the Late Cretaceous, the Aegean-Anatolian region has been characterized by ~2000 km of northward subduction at ~2 cm/year of the leading edge of Africa beneath Eurasia along the Hellenic subduction zone (Fig. 1). Cretaceous-to-Eocene subduction produced high-pressure/low-temperature (HP/LT) metamorphic rocks and arc volcanics that are currently exposed in parts of mainland Greece, the Cycladic Islands in the Aegean, and western Turkey. Slab retreat and regional extension began in the Eo-Oligocene and continues to the present (Royden, 1993; Jolivet et al., 2010b, 2013; Papanikolaou, 2013). Slab rollback through time has resulted in ~700 km southward migration of the magmatic arc, southward younging of subduction-related metamorphism and flysch sedimentation (Jolivet and Brun, 2010; Ring et al., 2010; Papanikolaou, 2013), and progressive exhumation of HP/LT rocks in the wake of the retreating slab in the backarc region (Ring et al., 2001; Jolivet et al., 2003; Ring and Glodny, 2010).

In the Cycladic Islands in the central Aegean, the multi-stage tectonic history is best recorded in the Cycladic Blueschist Unit (CBU). The CBU protoliths include Carboniferous orthogneissic basement; Mesozoic sediments, volcanics, and carbonate platforms; and Late Cretaceous (ca. 80–75 Ma) oceanic lithosphere (Bonneau, 1984; Tomaschek et al., 2003; Bröcker and Pidgeon, 2007; Tomaschek et al., 2008; Papanikolaou, 2013). These rocks record Eocene (ca. 53–40 Ma) HP/LT subduction-related deformation and metamorphism (Dixon, 1976; Okrusch and Bröcker, 1990; Tomaschek et al., 2003; Lagos et al., 2007; Skelton et al., 2018). The metamorphosed Cretaceous oceanic lithosphere, which was relatively young (~30 m.y.) and hot at the time of subduction, contains relict pillow lavas and Mn-rich metasediments characteristic of a magmatically and hydrothermally active oceanic crust (Keiter et al., 2004, 2011). However, some CBU serpentinites and chlorite schists retain oxygen isotopic and trace-element signatures that indicate serpentinization occurred on or beneath the seafloor before subduction (Cooperdock et al., 2018), suggesting they could have formed in a hyper-extended magma-poor rifted margin (e.g., Beltrando et al., 2014). Regardless of the specific geodynamic setting, the CBU juxtaposes a variety of protolith types that all experienced the Eocene high-pressure event. Subsequent greenschist-facies retrogression and deformation occurred during Oligo-Miocene exhumation along crustal-scale, low-angle normal faults of the North and West Cycladic Detachment Systems, the Paros-Naxos Detachment System, and the Santorini Detachment System (Avigad and Garfunkel, 1991; Forster and Lister, 1999; Ring et al., 2010; Jolivet et al., 2010b; Grasemann et al., 2012; Soukis and Stockli, 2013; Schneider et al., 2018). The CBU locally records an amphibolite-facies metamorphic event and migmatization of Miocene arc-related granitoid intrusions, best exposed on Naxos (Jansen, 1977; Andriessen et al., 1979).

Among the Cycladic Islands, HP/LT metamorphism is best preserved on Syros (Ridley, 1982; Trotet et al., 2001; Putlitz et al., 2005). From structural top to bottom, the CBU on Syros comprises an uppermost metabasite unit containing slivers of serpentinite that reached peak metamorphic conditions at ca. 53–50 Ma; several nappes of intercalated metasediments and marble schists (with mafic lenses) that reached peak conditions at ca. 43–38 Ma; and greenschist-facies gneisses and schists (Tomaschek et al., 2003; Keiter et al., 2004, 2011; Lagos et al., 2007; Skelton et al., 2018) (Fig. 1). The maximum pressure-temperature estimates for the CBU are quite variable in the literature (particularly with regard to pressure), ranging from ~14 to 23 kbar and ~450 to

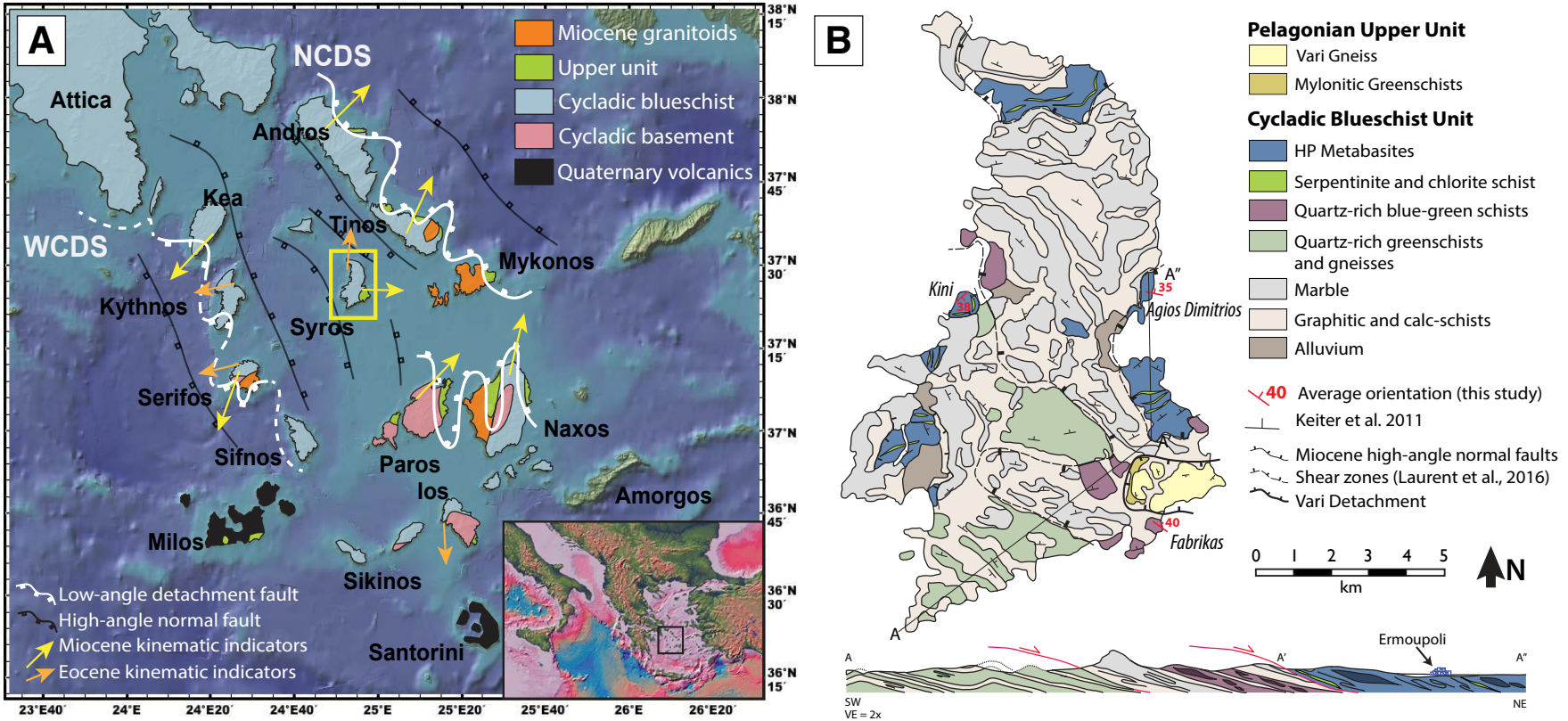

Figure 1. (A) Regional tectonic map of the Cyclades. Yellow box indicates Syros and area shown in (B) (modified after Grasemann et al., 2012). (B) Geologic map of Syros. Three localities discussed in this study are labeled (modified from Bröcker et al., 2013).

500 °C in the blueschist-to-eclogite facies (Fig. 2A) (Schliestedt, 1986; Putlitz et al., 2000, 2005; Trotet et al., 2001; Schmädicke and Will, 2003; Behr et al., 2018; Laurent et al., 2018). Reported pressures correlate to a maximum depth range between ~45–80 km, assuming lithostatic conditions. The structural evolution on Syros comprises at least two stages of penetrative foliation development and folding during subduction to peak depths, followed by progressive localization of strain under retrogressive blueschist- and eventually greenschist-facies conditions during exhumation (Fig. 2B; Dixon, 1976; Ridley, 1982; Rosenbaum et al., 2002; Keiter et al., 2004, 2011; Bond et al., 2007; Laurent et al., 2016). Additionally, the presence of undeformed lawsonite and aragonite pseudomorphs indicates penetrative strain in some meta-mafic exposures ceased at or near peak pressures and temperatures prior to exhumation (Keiter et al., 2004; Philippon et al., 2012).

Many observations suggest exhumation on Syros occurred in two stages: an initial stage in which rocks were returned from peak depths (~45–80 km) to the overriding forearc in a subduction channel geometry and a second stage in which rocks were exhumed from the middle crust (~20–30 km) along semi-brittle and brittle crustal-scale detachment faults and shear zones (Avigad et al., 1997; Jolivet et al., 2003, 2010b; Ring et al., 2010; Laurent et al., 2018; Fig. 2B). These stages are commonly distinguished by metamorphic grade and by the dominant orientation of mineral lineations: whereas prograde rocks preserve N-S–trending lineations consistent with the orientation of subduction, retrograde rocks preserve NE- and E-trending lineations (Gautier and Brun, 1994; Rosenbaum et al., 2002; Jolivet et al., 2013; Philippon et al., 2013; Laurent et al., 2016). Rb-Sr ages of phengites micro-drilled from exhumation-related fabrics in metasedimentary units indicate that deformation and metamorphism

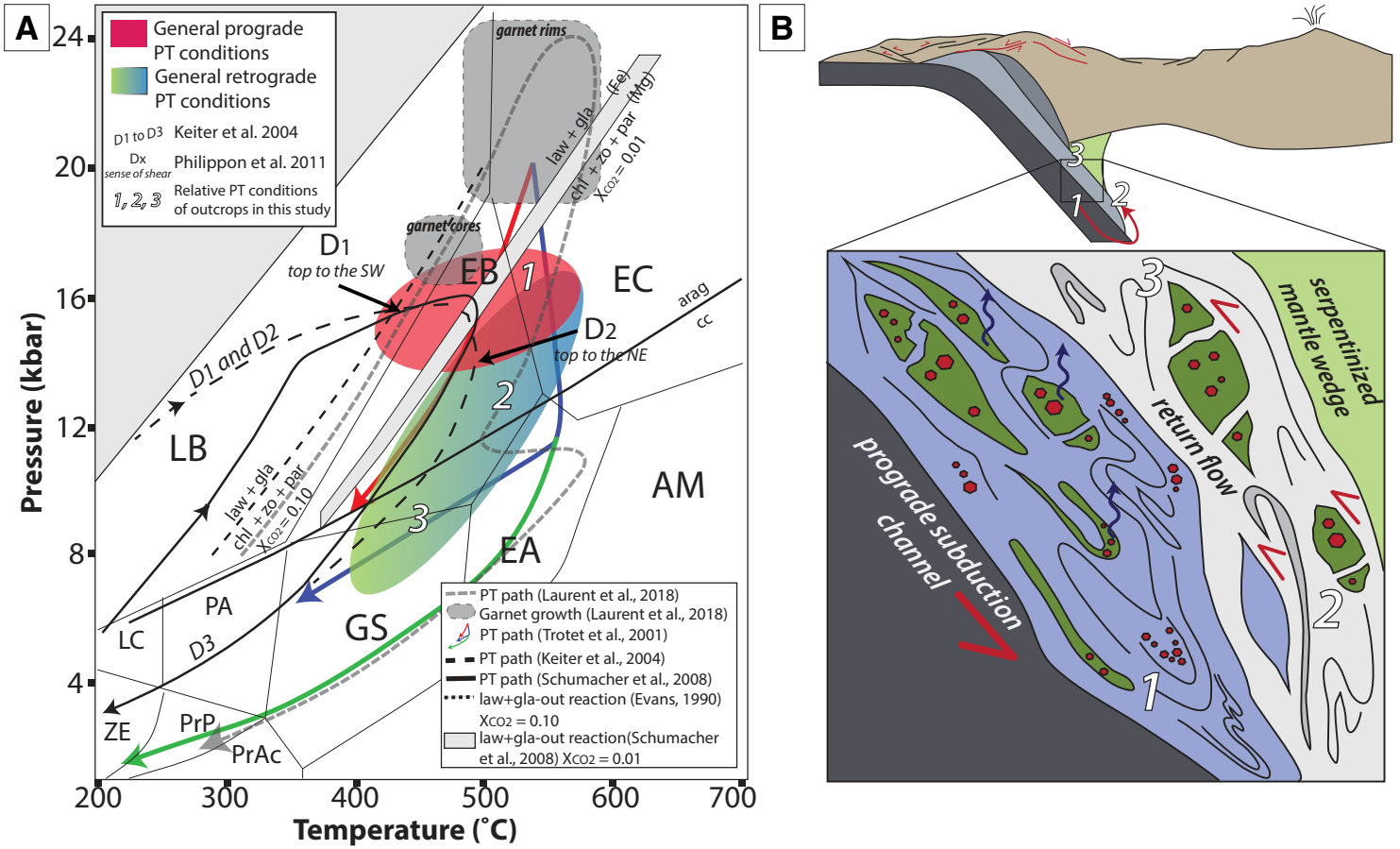

Figure 2. (A) Published pressure-temperature (PT) paths and interpreted deformation-metamorphism histories for Syros rocks. Pink and blue-green ovals and white numbers 1–3 indicate relative PT conditions of rocks addressed in this study for Kini, Fabrikas, and Agios Dimitrios, respectively. White numbers correspond to structural positions in (B), representative of (1) subduction, (2) return flow under blueschist-facies conditions, and (3) return flow under greenschist-facies conditions in the subduction shear zone or "channel." Abbreviations for metamorphic facies fields are as follows: ZE—zeolite; PrAc—prehnite-actinolite; PrP—prehnite-pumpellyite; LC—lawsonite-chlorite; PA—pumpellyite-actinolite; GS—greenschist; LB—lawsonite blueschist; EB—epidote blueschist; EA—epidote amphibolite; AM—amphibolite; EC—eclogite.

occurred continuously in the subduction channel as rocks exhumed between ca. 42–30 and perhaps even to 20 Ma (Bröcker et al., 2013; Cliff et al., 2017). The latest exhumation stages on Syros are best recorded by the Miocene Vari detachment, which crops out on the southeast tip of the island (Fig. 1B) and juxtaposes greenschist-facies mylonites and gneisses in the hanging wall against CBU in the footwall (Ring et al., 2003; Soukis and Stockli, 2013). This structure has been characterized as a reactivated subduction channel roof that assisted exhumation from ~500 to 550 °C in the eclogite facies, through ~450–500 °C in the blueschist facies during continuous subduction and early stages of slab rollback (Jolivet et al., 2010a; Laurent et al., 2016).

For this study, we selected three Syros exposures (Kini, Agios Dimitrios, and Fabrikas) that represent different subducted protoliths and different conditions of deformation within the subduction shear zone (Figs. 1 and 2). The Kini and Agios Dimitrios exposures were selected because they comprise dominantly oceanic-affinity meta-mafic rocks and thus may provide insight into the rheological behavior of subducted oceanic crust that is sediment poor. The Fabrikas locality is a heterogeneous lens of meta-mafic and metasedimentary rocks, itself contained within a surrounding matrix of calc-schists and marbles (Fig. 1). Therefore, this locality provides insight into the rheological behavior of subducted oceanic crust blanketed by sediment. For each exposure, in Section 3, we first provide a general description of the outcrop characteristics and then summarize the interpreted pressure-temperature (PT) conditions recorded there, based on both previously published work and our own observations. We then describe the types of rheological heterogeneities preserved at each locality, where heterogeneities are defined as any features that produce outcrop-scale strain gradients or significant differences in deformation mode or mechanism. We document the types, sizes, and distributions of rheological heterogeneities based on field measurements and the deformation mechanisms that define the heterogeneous materials using microstructural observations (all measurements are provided in Supplemental Tables S1–S4[1]). In Section 4, we discuss our observations in the context of (1) the sources of rheological heterogeneity that exist and/or persist at depth in generalized subduction settings; (2) the mechanical behavior of the deep interface; and (3) the compatibility of the observed rheological heterogeneities and their deformation modes with observations and models of ETS in modern subduction zones.

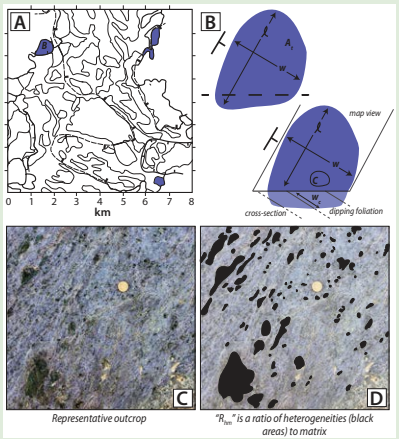

3. THREE EXPOSURES ON SYROS

3.1 Kini

The Kini area, part of the structurally highest oceanic-affinity subunit, spans ~400 m of coastal exposure where meta-mafic blueschists and eclogites are exceptionally exposed. The protolith is dominantly Late Cretaceous mid-ocean ridge basalt, with some rocks preserving a more calc-alkaline signature (Bonneau, 1984; Seck et al., 1996; Tomaschek et al., 2003; Bulle et al., 2010). Map-scale slivers of serpentinite and chlorite-talc schist are mostly localized to the Kini block's margins (Fig. 1). In-place exposures are cliffs several tens of meters in height, comprising alternating glaucophane-garnet-epidote blueschists, minor chlorite-talc schists, and interspersed pods of eclogite containing omphacite + garnet ± glaucophane, and zoisite. Foliations dip gently to moderately S-SE and exhibit tight to isoclinal folds with axial planes subparallel to the foliation. These folds are visible on the centimeter to meter scale in outcrop and have moderately S-plunging fold axes commonly decorated by mineral lineations defined by glaucophane, epidote, and phengite (Fig. 3A). Locally, the primary foliation is cut by an upright crenulation cleavage with NE-SW–striking axial planes associated with some realignment and growth of glaucophane, epidote, and phengite.

3.1.1 Interpreted PT Conditions

The primary foliation at Kini is interpreted to record prograde subduction and/or peak metamorphic temperature within the subduction shear zone based on (1) preservation of N-S–trending lineations in HP minerals, which is consistent with the orientation of prograde shearing (Philippon et al., 2013; Laurent et al., 2016; Behr et al., 2018); (2) preservation of undeformed lawsonite pseudomorphs stamped over the foliation or only weakly deformed (Keiter et al., 2004, 2011; Philippon et al., 2013); and (3) a lack of retrogressive phases or extensive mineral replacement (Behr et al., 2018). We reason that the upright crenulation cleavage likely developed in the early stages of exhumation since it overprints an older foliation and represents a rotation of maximum compressive stress by ~90°. This transition in principal stress orientation would not be expected if rocks were being sheared along a continuous path during subduction.

3.1.2 Rheological Heterogeneities

We document two primary types of heterogeneities at Kini: (1) coarse-grained blueschist-to-eclogite facies gabbroic pods; and (2) fine-grained, massive to weakly foliated eclogite lenses. The coarse-grained meta-gabbro pods have massive textures that resemble igneous cumulates, characterized by blueschist-facies minerals glaucophane, epidote, garnet, ± omphacite (Figs. 4A and 4B). The surrounding matrix rocks are fine grained, strongly foliated, epidote-blueschist–facies meta-basalts that wrap around the meta-gabbros, producing boudin-matrix structures. Meta-gabbro pods range from ~5 cm to 5 m in equivalent circle diameter, with aspect ratios (stretching-parallel length to foliation-perpendicular width) on average ~1.5:1 (Fig. 3B). The interiors of meta-gabbros are unstrained to weakly foliated; weak fabrics are visible in preferentially aligned epidote. Some metamorphosed pods preserve weak shearing of relict intrusive relationships in which finer-grained mafic rocks are juxtaposed with the coarser-grained gabbros (Fig. 4A). The second type of heterogeneity at Kini is associated with local concentrations of eclogite-facies minerals in discrete lenses, pods, and boudins embedded within the blueschist matrix (Figs. 4C–4G).

[1]Supplemental Material. Structural data characterizing rheological heterogeneities, and details for calculations of effective source areas and equivalent seismic moments of tremor bursts. Please visit https://doi.org/10.1130/GES02037.S1 or access the full-text article on www.gsapubs.org to view the Supplemental Material.

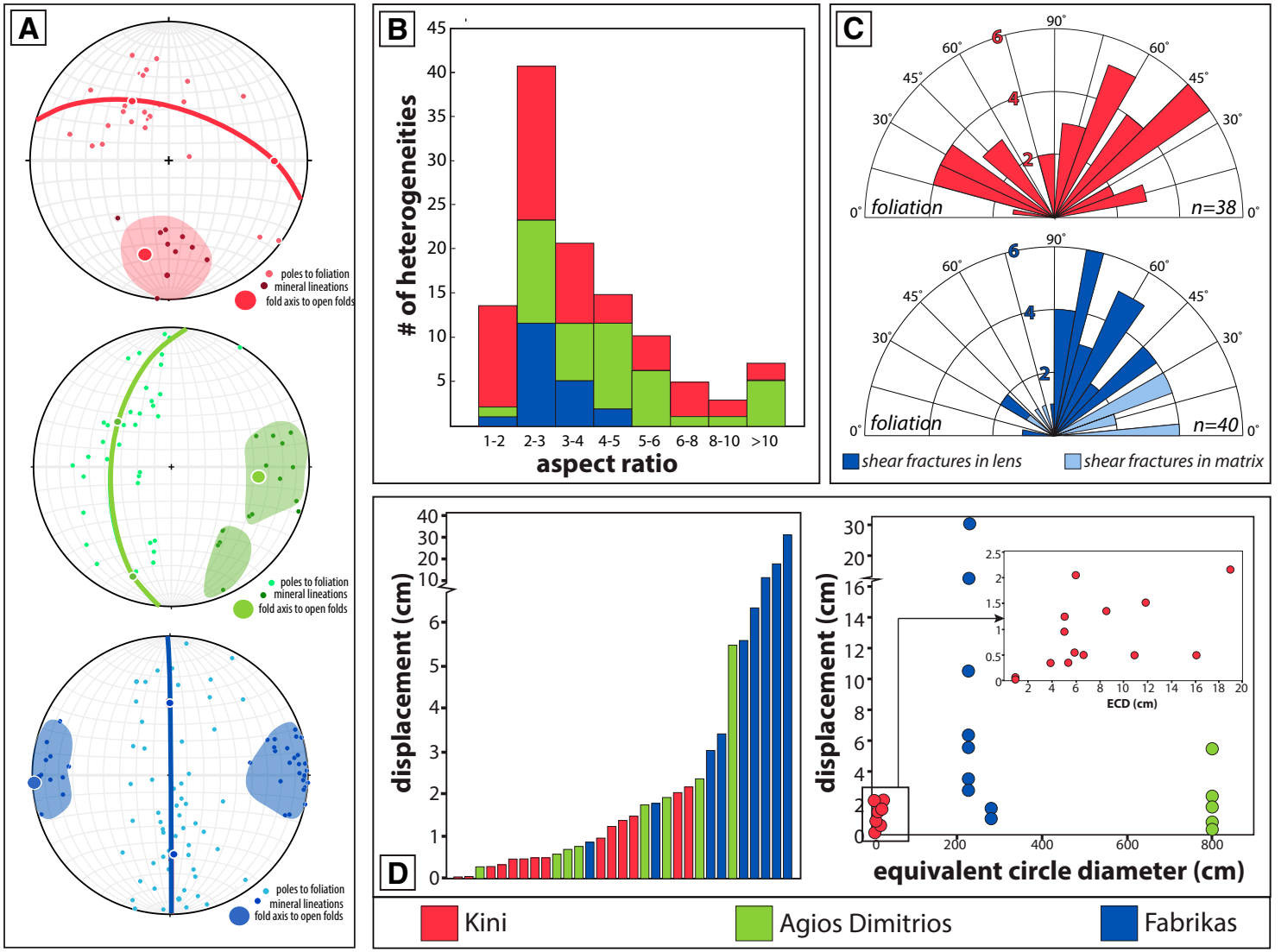

Figure 3. Compilation of outcrop structural data and characteristics of heterogeneities. Red—Kini; green—Agios Dimitrios; and blue—Fabrikas. (A) Equal-area, lower-hemisphere projection stereoplots of poles to foliation, best-fit great circles of poles to foliation (heavy colored lines), and fold axes to open folds (heavy circles). Colored patches outline mineral lineation orientations. (B) Histogram of eclogite aspect ratios demonstrating that the majority show low aspect ratios consistent with low amounts of ductile strain relative to the matrix. (C) Rose diagrams of angles between fractures and/or veins and foliation for Kini and Fabrikas, illustrating the presence of optimally oriented shear and Mode I fractures in strong pods. (D) Range of eclogite displacement magnitudes (left) and equivalent circle diameters (ECDs) of eclogites versus displacement for each locality. Zoom-in shows distribution of Kini eclogite data. Displacement measurements in (D) will be used in calculations shown in Section 4.3. See Supplemental Material (footnote 1) for table of displacement measurements.

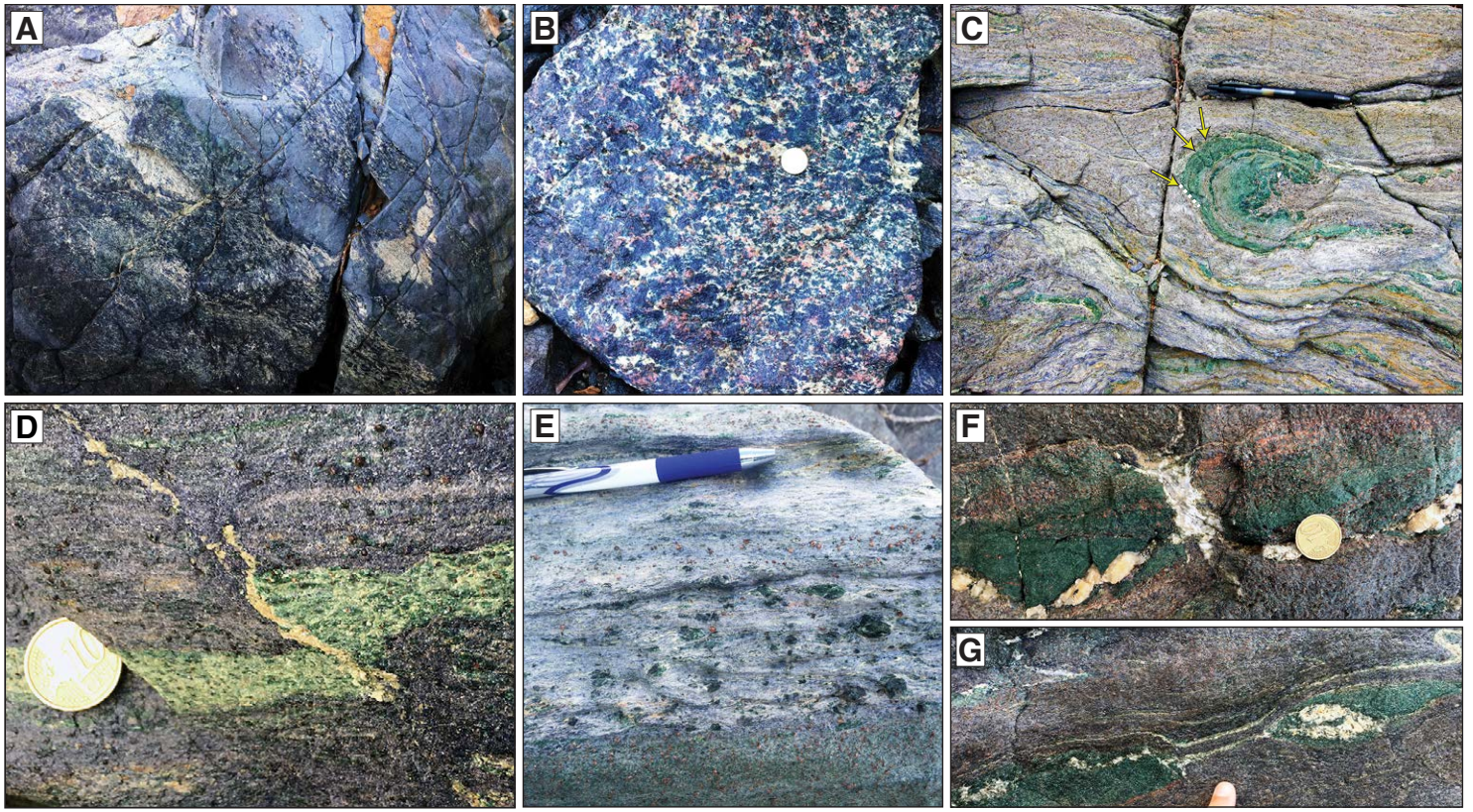

Figure 4. Representative field photos from Kini. (A, B) Blueschist-eclogite–facies meta-gabbros with igneous textures preserved. (C) Folded eclogite lens in blueschist matrix with brittle shear fractures dissecting the nose of the fold (37°26′42.8″N, 24°53′20.5″E). Arrows point to shear fractures. (D) Shear fracture filled with quartz through an eclogitic foliation-parallel lens. We measured brittle offset in eclogite pods by reconstructing piercing points of the offset eclogite features; for examples, see (C) and (D). (E) Omphacite pods decorating the blueschist foliation on the cm scale. (F) Eclogite lens with older quartz veins sheared into the foliation and brittlely offset, and a younger phengite-quartz vein opening perpendicular to blueschist foliation. (G) Pinched quartz-filled boudin neck in eclogite lens.

The largest eclogite pods are fallen blocks along the coastline up to tens of cubic meters in volume. The majority of eclogite lenses that are observed in place, however, range from 0.5 to 20 cm in equivalent circle diameter with average aspect ratios of 2.5:1–3.5:1 (Fig. 3B). The smaller eclogite pods are typically distributed on the centimeter to tens of centimeters scale throughout the local matrix, whereas larger ones are commonly separated from one another by several meters. Several of the eclogitic lenses can be classified as fractured boudins, where the fractures are dilational veins opened perpendicular to the foliation (Figs. 4F,4G, and 5). Dilational shear fractures are also common, occurring at 30°–55° angles to the foliation, and some filled with quartz, phengite, glaucophane, and/or chlorite (Figs. 3C, 4C, 4D, 4F, 4G, 5A, and 6A). Displacements on shear fractures range from 0.1 to 2.0 cm (Fig. 3D and Table S3 [footnote 1]). In some places, an earlier generation of veins appears sheared into parallelism with the surrounding matrix and is cut by later-generation veining oriented at higher angles to the foliation (Figs. 4F and 4G). Some mineralized veins filling boudin necks are themselves boudinaged (Fig. 4G). The veins and shear fractures are most prominent in omphacite- and garnet-rich eclogitic lenses, whereas eclogite pods with greater concentrations of glaucophane and/or epidote are instead weakly folded at a greater wavelength than the surrounding blueschist matrix, and fractures are less well developed. In nearly all examples, the dilational veining and shear displacement that occur within the eclogitic lenses are accompanied by ductile flow in the surrounding blueschist matrix (Figs. 4C–4G).

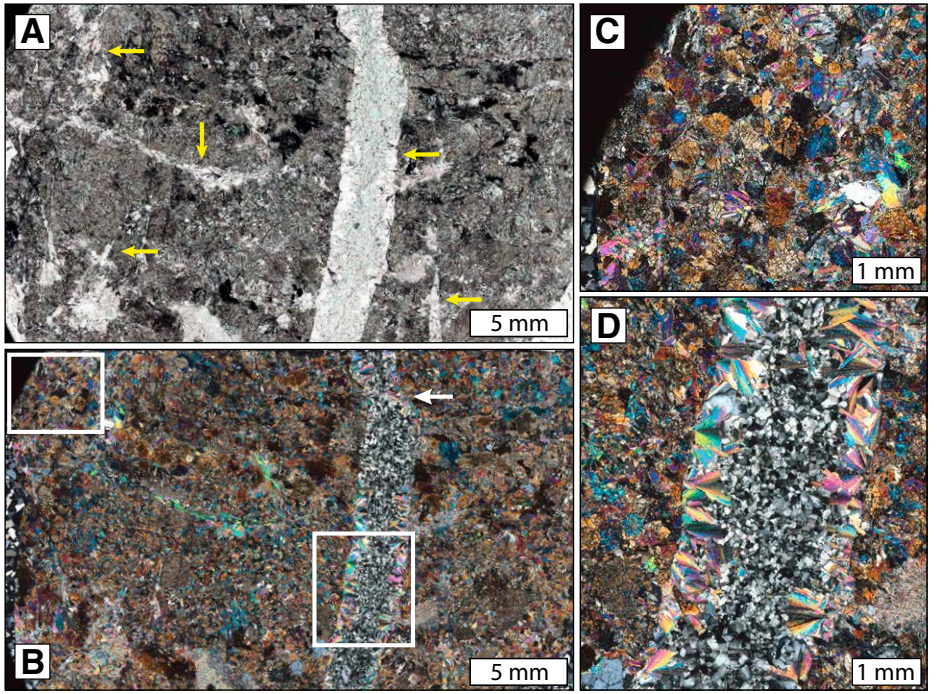

Figure 5. (A, B) Massive veined eclogite microstructure in plane-polarized light (PPL) (A) and cross-polarized light (XPL) (B). Yellow arrows in (A) show brittle and semi-brittle veins filled with phengite, and white arrow in (B) shows weak shearing after vein emplacement. White boxes in (B) correspond to images to the right showing (C) cumulate meta-gabbroic texture and abundant intracrystalline fracture in omphacite and (D) showing a vein filled with high-pressure chlorite and radiating phengite crystals.

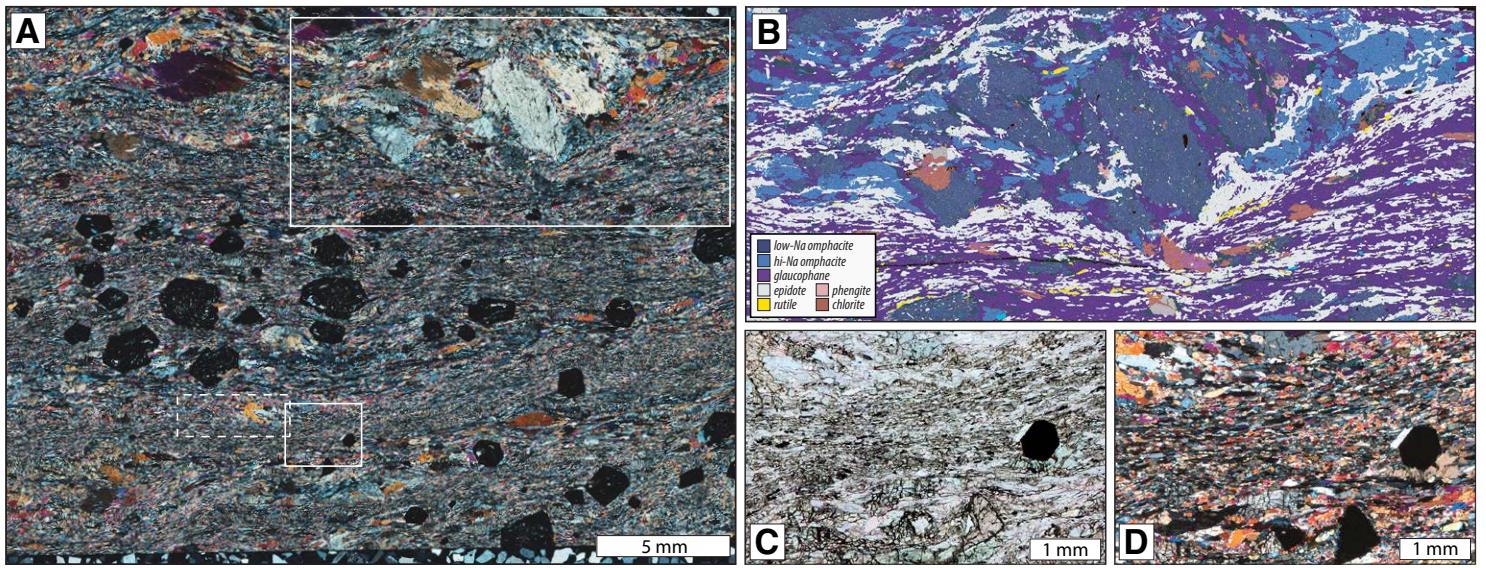

Figure 6. (A) Representative blueschist microstructure at Kini; fine-grained glaucophane and epidote matrix with large garnet and semi-brittle omphacite porphyroblasts. Dashed white box correlates to EBSD map shown in Figure 7. (B) False-colored X-ray map of area outlined with large white box in (A). Note higher-Na omphacite in pressure shadows fringing the lower-Na omphacite porphyroblast, and filling in dilational fractures. (C, D) Zoom in to small white box in (A) showing omphacite-epidote blueschist in plane-polarized light (PPL) (C) and cross-polarized light (XPL) (D). Note through-going intracrystalline fractures in garnets and epidote in coarse-grained sections. Fine-grained epidote and glaucophane define a strong foliation and develop prismatic and diamond-shaped subgrains and newly recrystallized grains, best seen in XPL (D).

3.1.3 Microstructural Observations

In thin section, Kini blueschists consist of alternating glaucophane- and epidote-rich layers with porphyroblasts of omphacite, phengite, garnet, rutile, and minor quartz, titanite, and chlorite. Glaucophane and epidote grain sizes range from 50 to 500 µm, and porphyroblasts of garnet and omphacite range from 300 µm–5 mm (Fig. 6A). Omphacite porphyroblasts comprise two chemically distinct types: a high-Mg, low-Na core, fringed by a low-Mg, high-Na tail. In Figure 6B, a low-Na omphacite porphyroblast is brittlely sheared and offset by micro-domino fractures. Brittle fractures have a component of dilation and are filled with glaucophane and high-Na omphacite. In Figure 7, we show electron backscatter diffraction (EBSD) data to quantify intracrystalline strain and lattice-preferred orientation (LPO). Glaucophane and epidote preserve evidence of intracrystalline plasticity in the form of undulose extinction, subgrain walls oriented both parallel and perpendicular to the foliation, bulging grain boundaries, newly formed strain-free grains (~100 µm), and strong LPOs. For description of electron micro-beam methods, please see Supplemental Text (footnote 1). Behr et al. (2018) also presented EBSD data from two Kini blueschists with similar results. The eclogites at Kini are primarily massive in texture, with grain sizes ranging from 300 µm–1 mm. As observed at the field scale, the eclogites are commonly cut by multiple generations of veins filled with white mica ± chlorite and quartz (Figs. 5A–5D).

3.2 Agios Dimitrios

Agios Dimitrios, just north of Ermoupoli on the east coast of Syros, is another exposure of the structurally highest oceanic-affinity blueschist-eclogite subunit. Similar to Kini, the outcrop spans ~900 m of coastline and is continuous over several tens of meters in height and length. The primary foliation is characterized by intercalated fine-grained blueschist and chlorite-actinolite greenschist, with lenses of omphacite-garnet ± glaucophane, epidote eclogite. Blueschist and greenschist foliations are folded, with a shallowly E-plunging fold axis. Mineral lineations in glaucophane and epidote plunge dominantly E, but S- and SE-plunging lineations are also present (Fig. 3A).

3.2.1 Interpreted P-T Conditions

The dominant phase of deformation and metamorphism at Agios Dimitrios is interpreted to record return flow in the subduction shear zone from eclogite facies down pressure and temperature into greenschist-facies conditions. This interpretation is based on (1) preservation of some S-trending, but dominantly SE- and E-trending lineations in HP and greenschist-facies minerals (Fig. 3A), which we interpret to represent a progressive change in stretching direction from subduction to exhumation; (2) preservation of foliation-parallel, coexisting blueschist-facies and greenschist-facies mineral assemblages (cf. Fig. 8); (3) partial replacement of eclogites by epidote and glaucophane (Fig. 9).

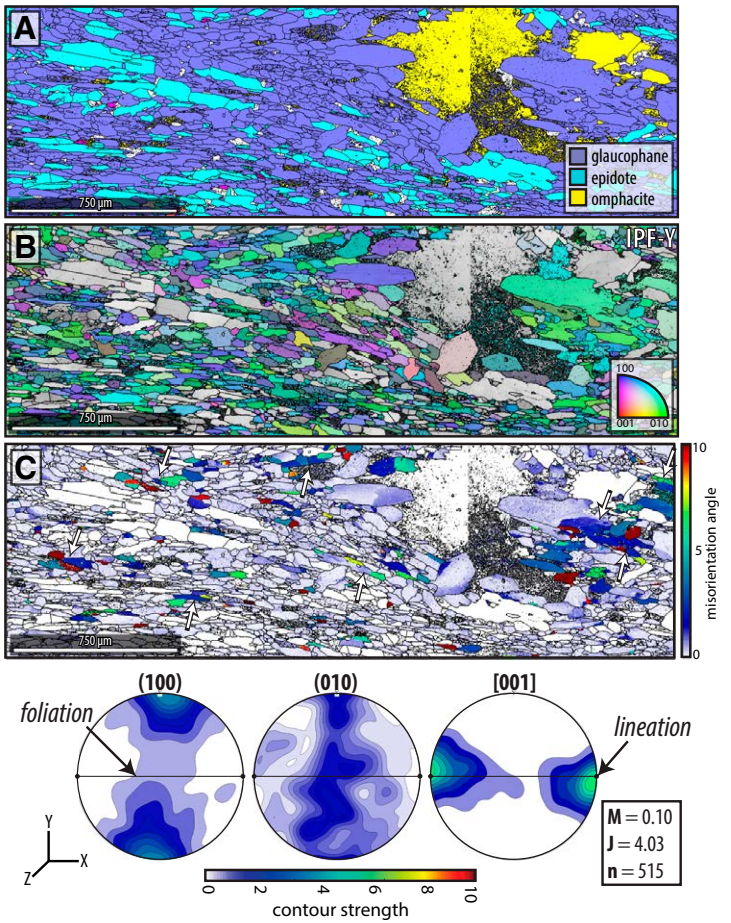

Figure 7. Electron backscatter diffraction (EBSD) maps of Kini blueschist (sample KCS16K). (A) Phase map; (B) Inverse pole figure (Y-vector) map for glaucophane, with inset color-coded key. The similar blue-purple colors indicate that (100) crystallographic planes are mostly parallel to the Y-direction in the assigned reference frame (vertical, perpendicular to foliation). The green-yellow colors indicate that some (010) crystallographic planes are also parallel to Y-direction (also see pole figure below). (C) Misorientation map (Mis2Mean) showing intracrystalline plastic strain and subgrain formation in glaucophane, with color bar showing degrees of intracrystalline misorientation (°). White arrows point to areas that best highlight subgrain structure and porphyroclasts with surrounding recrystallized grains. Pole figure shows glaucophane lattice-preferred orientation (LPO) for (100) and (010) crystallographic planes and [001] direction. Pole figures are point per grain. Fabric strengths were calculated using the M and J indices as indicated (Skemer et al., 2005; Bunge, 1982). n—number of grains reported.

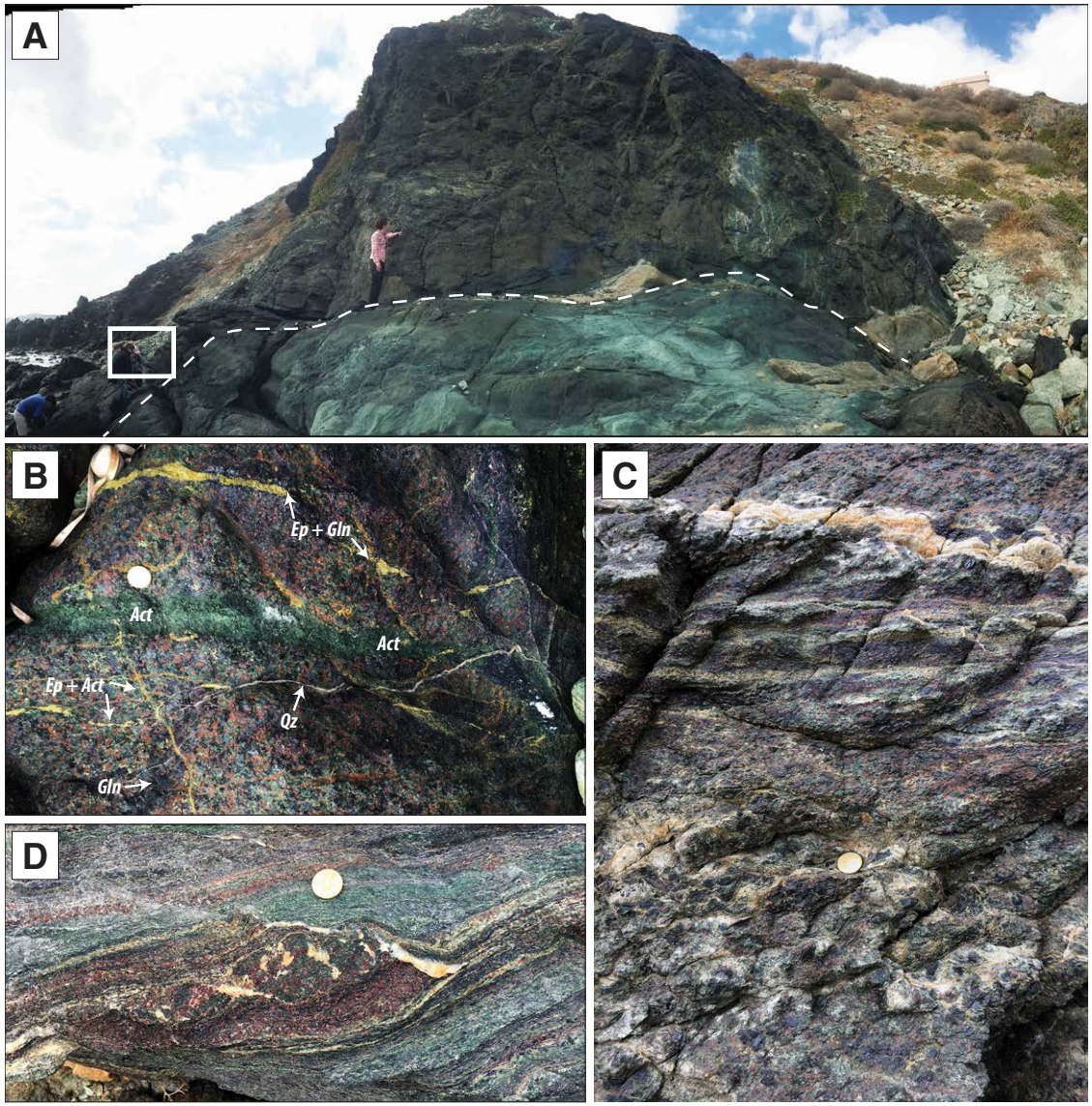

Figure 8. Representative field photos from Agios Dimitrios. (A) Eclogitic meta-gabbro (37°27′5.86″N, 24°56′56.92″E) encased in fine-grained actinolite-chlorite schist. Contact outlined in dashed white line. Person for scale is 1.5 m. White box corresponds to (B). (B) Massive meta-gabbro with cumulate texture crosscut by brittle veins filled with hydrous minerals. Dark inky blue is glaucophane; yellow is epidote; green is actinolite; white is quartz. (C) Massive meta-gabbro crosscut by quartz and epidote veins. The eclogitic pod is affected by viscous strain in the proximity of the veins. (D) Eclogitic lens dissected by quartz-filled shear fractures surrounded by blueschist-greenschist matrix. For our displacement measurements, we used features like offset veins (B) and eclogite lenses (D).

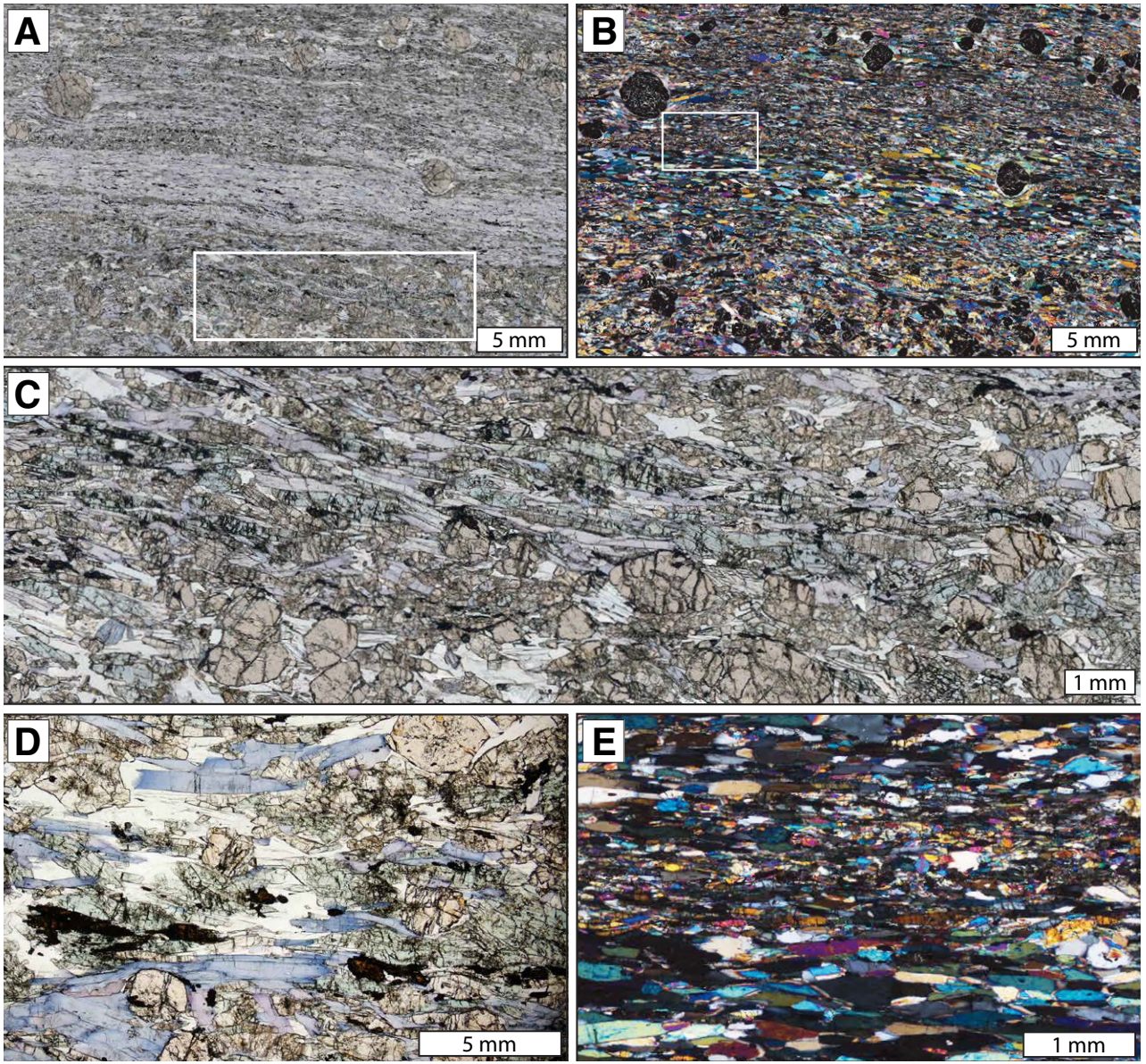

Figure 9. Representative photomicrographs of Agios Dimitrios microstructures. (A, B) Contact between garnet-epidote-blueschist and eclogite lens in plane-polarized light (PPL) (A); (white box corresponds to area in [C] and cross-polarized light (XPL) (B); (white box corresponds to area in [E] [section is 60 µm thick]). (B) Blueschist foliation is defined by glaucophane and epidote with consistent, fine-grain sizes with some undulose extinction. (C) Semi-brittle deformation in eclogite lens, with through-going intracrystalline fractures in omphacite and garnet. (D) Glaucophane replacing and growing over omphacite. (E) Glaucophane and epidote showing some undulose extinction and subgrain formation. Finer recrystallized grains are relatively strain-free.

3.2.2 Rheological Heterogeneities

Similar to Kini, the primary types of heterogeneities at Agios Dimitrios include: (1) coarse-grained blueschist-to-eclogite–facies meta-gabbros and (2) eclogitic lenses embedded in the surrounding matrix (Fig. 8D), but as discussed in Section 3.2, this unit has been partially retrogressed under blueschist-greenschist–facies conditions. We document a distinct meta-gabbro lens, which, like those described at Kini, preserves a coarse-grained massive texture resembling an igneous cumulate with omphacite, garnet, glaucophane, ± epidote (Fig. 8A). The surrounding matrix wraps around the eclogitic meta-gabbro and consists of fine-grained greenschists. This meta-gabbro is the largest heterogeneity of its type that we have yet found, standing ~5 m tall, ~10 m wide, and at least several m in the stretching-parallel direction, equating to a minimum volume of ~150 m^3. Because the view in Figure 8A is looking roughly parallel to lineation, it is difficult to determine a true aspect ratio, but the ratio of long:short axes in this view is ~2:1. This eclogitic meta-gabbro lacks a pervasive internal fabric and is dissected by multiple generations of dilational veins filled with a variety of hydrous phases (Figs. 8B and 8C). Crosscutting relationships indicate that epidote ± garnet veins rimmed with glaucophane are oldest; they are crosscut and in some places offset by later epidote ± glaucophane veins that are commonly rimmed by actinolite. All early veins are crosscut by actinolite- and/or quartz-filled veins, suggesting these are the youngest generation (Fig. 8B). Locally, splaying epidote-filled veins rimmed with actinolite appear to have been ductilely sheared to low strain during or after emplacement (Fig. 8C). The second type of heterogeneity at Agios Dimitrios, like at Kini, are local concentrations of eclogite-facies minerals in pods and lenses smeared and boudinaged within the mafic blueschist matrix (Fig. 8D). Pod sizes typically range from ~1–50 cm in equivalent circle diameter with average aspect ratios of 3:1–5:1; some elongated lenses are traceable parallel to the stretching direction for several meters with aspect ratios up to 15:1 (Fig. 3). Eclogite pods in the tens of cm size range are typically distributed within the matrix on a sub-cm to cm scale, whereas elongated eclogite lenses are distributed on the tens of cm to several meters scale. Brittle fractures in eclogite pods are observed (e.g., Fig. 8D), and ductile strain in eclogites is also common. Many of the lenses preserve pinch-and-swell textures or are folded at wavelengths slightly greater than the folds within the matrix blueschists.

3.2.3 Microstructural Observations

Similar to Kini, the Agios Dimitrios blueschists consist of alternating glaucophane and epidote-rich layers and porphyroblasts of garnet, phengite, rutile, chlorite, and minor quartz and titanite (Fig. 9). Local concentrations of eclogitic minerals omphacite and garnet are contained within the blueschist foliation and appear to be in textural equilibrium with the surrounding blueschist in some samples, whereas in others, glaucophane (±white mica) appears to be replacing and/or overgrowing brittlely distended crystals of omphacite (Figs. 9A–9C). Glaucophane and epidote grain sizes range from 100 µm–2 mm, and porphyroblasts of garnet and omphacite range from 400 µm–2 mm (Fig. 9). Glaucophane and epidote preserve evidence for intracrystalline plasticity similar to Kini blueschists, including weak undulose extinction, grain-size reduction to a uniform size of ~250 µm, and subgrain boundaries in larger ~1-mm-sized crystals oriented parallel and perpendicular to the foliation (Fig. 9).

3.3 Fabrikas

Fabrikas is an exposure of the middle subunit and is composed of blueschist-to-greenschist–facies metabasites, quartz-rich schists, and marbles. This mixed marble-metabasite-schist sequence is derived from Triassic–Jurassic rift-related volcanics and passive margin sediments (Bonneau, 1984; Bröcker and Pidgeon, 2007; Papanikolaou, 2013). The outcrop we focus on spans 25 m along the southeast Syros coastline, but similar exposure continues for ~600 m. Outcrops similar to Fabrikas are peppered throughout a dominantly marble and calc-schist matrix that occupies the majority of the island (Fig. 1). The Fabrikas locality is preferentially eroded by waves, resulting in a unique exposure of relatively resistant, coarse-grained meta-mafic pods that physically stand out from the surrounding, more strongly eroded fine-grained matrix of alternating blueschist and quartz-mica schist. Blueschist and quartz-schist foliations dip gently to moderately to the N, and poles to foliations define girdles that are roughly N-S, with fold hinges shallowly plunging E-W (Fig. 3A). An outcrop-scale extensional fabric is well developed, such that meta-mafic lenses and matrix rocks both preserve strong E-trending, shallowly plunging glaucophane mineral lineations (Fig. 3A), and all rock types preserve strong, asymmetric top-to-the-E senses of shear (Figs. 10A–10D). Similar lithologies and structural relationships are seen at the Delfini peninsula (west-central coastline), although matrix rocks at Delfini are dominantly greenschist.

3.3.1 Interpreted PT Conditions

As at Agios Dimitrios, Fabrikas records deformation during subduction to eclogite facies now preserved in local pods and lenses, but the majority of the outcrop-scale structural features likely record significant strain under retrograde blueschist-to-greenschist–facies conditions. This interpretation is based on: (1) preservation of eclogite-facies lenses encased in a blueschist matrix; these lenses are affected by incipient greenschist-facies mineral replacement (Ridley, 1982; Rosenbaum et al., 2002; Bond et al., 2007); (2) E-W–trending mineral lineations and fold hinges consistent with Eocene exhumation-related kinematics (Gautier and Brun, 1994; Jolivet et al., 2013; Laurent et al., 2016); (3) retrogressive blueschist-facies dilational shear veins crosscutting eclogite pods (this study, Figs. 10A and 10B); and (4) its structural position immediately beneath the Vari detachment, interpreted as the "subduction channel roof" during early stages of exhumation (Laurent et al., 2016).

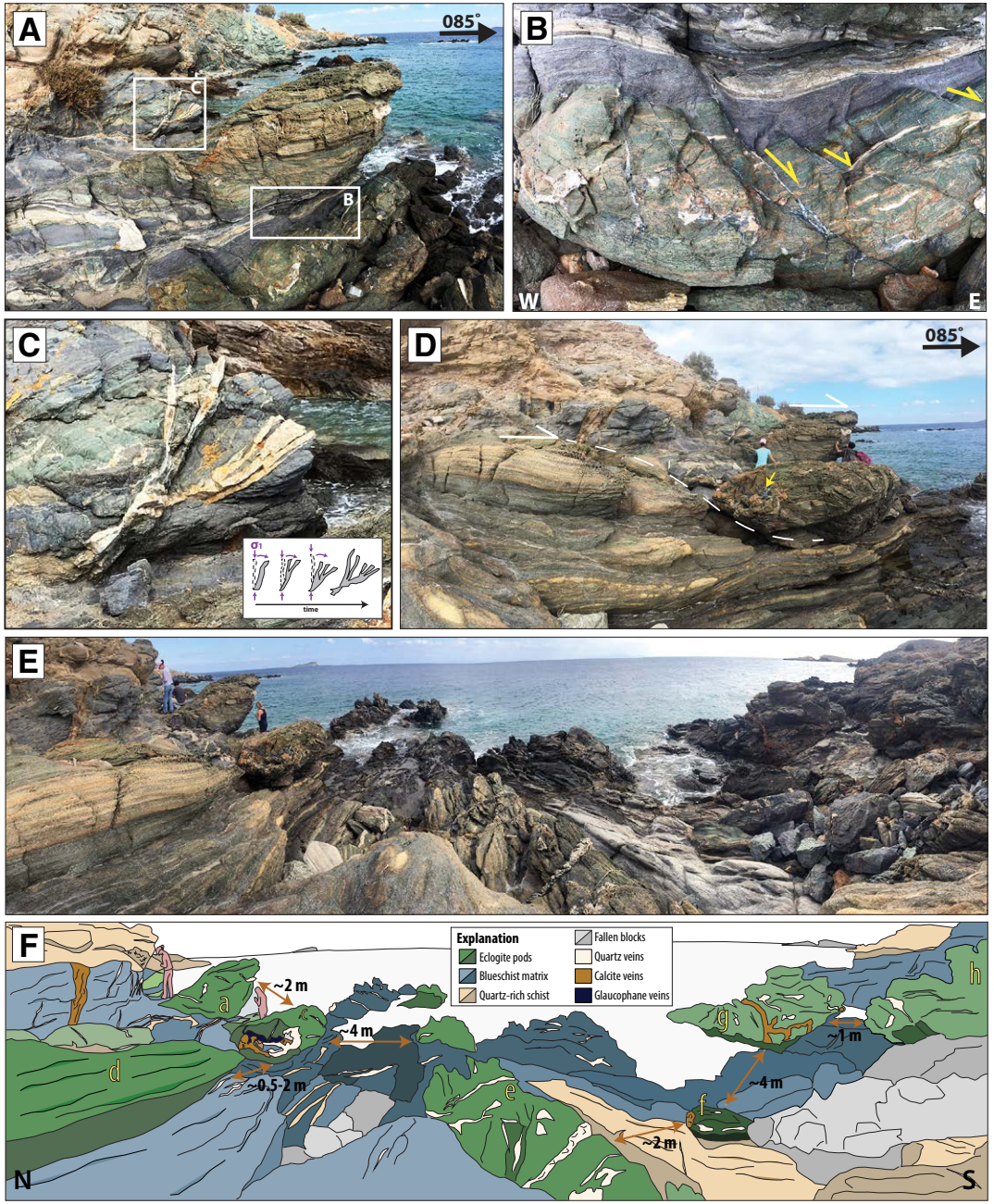

Figure 10. Representative field photos from Fabrikas. (A) Eclogite fish (~4 m in length) with top-E sense of shear in quartz schist and blueschist matrix. (B) Margin of an eclogite pod dissected by brittle shear veins filled with glaucophane and quartz, continuous with viscous shear bands in surrounding blueschist and quartz-schist matrix. We measured brittle shear offsets along discrete fractures like those shown in (B). (C) Series of quartz veins showing evidence for alternating injection into surrounding matrix rocks and subsequent shear (see inset in bottom right for interpretation). (D) Shear-band boudinage through eclogite lens showing top-E sense of shear. Yellow arrow points to glaucophanite vein material filling the eclogite boudin neck. (E) Panoramic photo of Fabrikas outcrop and eclogite heterogeneities, looking east (088°); see (F) for interpretation and explanation.

3.3.2 Rheological Heterogeneities

Similar to Kini and Agios Dimitrios, heterogeneity at Fabrikas occurs as meta-mafic lenses encased within the surrounding matrix, except in this case, the matrix is dominantly metasedimentary. As at Agios Dimitrios, the rocks at Fabrikas are retrogressed to blueschist-greenschist facies. Because of the unique exposure at Fabrikas, heterogeneities could be measured in three dimensions. The meta-mafic lenses range in equivalent circle diameter from ~5 cm to 4 m, corresponding to tens of cm^3 to tens of m^3 in volume, with the majority of pods in the ~1–15 m^3 range (Fig. 3D), and aspect ratios typically ranging between 2:1:1 and 3:1:1 (l:w:h) (Fig. 3B and Fig. 10). Spatial distributions commonly have two modes: pods in the less than tens of cubic centimeters range are separated by cm to several m, and pods in the less than tens of cubic meters range are separated by tens of centimeters to several meters, both along the stretching direction and within the plane of the foliation (Figs. 10D and 10E). Many of the meta-mafic lenses are fractured boudins. Mineralized boudin necks are oriented nearly perpendicular to the surrounding matrix foliation, and pods are crosscut by multiple generations of dilational veins and mineralized shear fractures, oriented at 35°–65° angles to the foliation and filled with quartz, glaucophane, phengite, ± actinolite and chlorite (Figs. 3C, 3D, and 10). Displacements on dilational shear fractures range from ~1 cm to ~25 cm (Fig. 3D) but are usually in the cm range. In most pods, an earlier generation of quartz veins has been transposed into parallelism with the internal eclogite foliation; these older veins are crosscut by the younger, higher-angle veins (Fig. 10B). Brittle fractures in eclogites are commonly continuous with viscous shear bands in the surrounding blueschist- and quartz-schist matrix (Fig. 10B). In some places, quartz veins cut through matrix rocks near the margins of eclogite pods and preserve at least three generations of vein injection followed by progressive rotation into the foliation (Fig. 10C).

3.3.3 Microstructural Observations

The matrix at Fabrikas comprises layers of garnet-mica-quartz schists and garnet-omphacite blueschists that alternate on the centimeter to decimeter scale. The quartz-rich schists preserve alternating ~1-mm-thick layers of white mica and quartz, with grain sizes ranging from 40 to 400 µm (Fig. 11). C′ shear bands decorated with recrystallized phengite, paragonite, and chlorite are commonly developed in more micaceous regions. Porphyroblasts of glaucophane and epidote 200 µm–5 mm are aligned within the foliation, and garnets 400 µm–12 mm in size are dispersed throughout (Figs. 11A and 11B). Glaucophane and epidote crystals are commonly brittlely boudinaged and partially replaced by green amphibole and/or chlorite (Figs. 11A and 11B). In Figure 12, we present EBSD data for one quartz-mica schist and one blueschist from Fabrikas. Quartz aggregates preserve moderate shape-preferred orientations and abundant evidence of intracrystalline plasticity in the form of sweeping undulose extinction, subgrain formation at multiple orientations, highly irregular or "amoeboid" grain boundaries, new, small, recrystallized grains, and a moderate-strength lattice-preferred orientation indicative of basal <a>, rhomb <a>, and prism <a> slip under plane strain conditions. The blueschists are dominantly glaucophane, omphacite, and epidote, and minor phengite, rutile, and calcite, with grain sizes between 150 µm–1 mm. Poikiloblastic garnet and epidote range in size from 1 to 3.5 mm (Figs. 11D and 11E). Epidote porphyroblasts are both aligned parallel to the matrix and rotated obliquely within the foliation. Garnet and epidote porphyroblasts contain inclusions of omphacite and glaucophane. As at Kini and Agios Dimitrios, the matrix preserves evidence for intracrystalline plasticity in glaucophane and epidote in the form of undulose extinction, subgrain walls oriented both parallel and perpendicular to the foliation, bulging grain boundaries indicative of grain boundary migration, and strong LPOs (Fig. 12).

4. DISCUSSION

4.1 Sources of Heterogeneity on the Deep Interface

Our observations from Syros highlight two sources of rheological heterogeneity: (1) variations in rock type in the subducted protoliths; and (2) more minor textural and geochemical variations in a single oceanic-affinity protolith that are amplified during metamorphism (Fig. 13).

The cumulate-textured gabbroic pods at Kini and Agios Dimitrios are examples of textural variations that are inherited from the oceanic protolith and that persist to at least 50 km depth. Prior to subduction, fine-grained extrusive volcanic rocks and sheeted dikes close to the seafloor are highly altered by high-temperature, amphibole-bearing hydrothermal veins (up to ~10% by volume) and weakened by low-temperature clay minerals and (sub) greenschist-facies metamorphism (Bach et al., 2003; Schramm et al., 2005). In contrast, coarse-grained lower-crustal gabbros record significantly less alteration by high-T phases than the upper volcanics (up to ~2% by volume), and only achieve low-T alteration in local zones of high fracture intensity (Bach et al., 2001). Therefore, the weaker uppermost volcanics likely localize strain early on in their subduction history (e.g., Rubie, 1983; Hacker, 1996), permitting the stronger coarser-grained gabbros to persist as rigid clasts within the weaker matrix (Fig. 13, insets C and D). Examples of meta-gabbros in a more deformed, fine-grained mafic or ultramafic matrix are preserved in many other exhumed subduction shear zones globally, suggesting that this form of heterogeneity on the deep interface may be quite common (e.g., Kurz et al., 1998; Rawling and Lister, 2002; Angiboust et al., 2011). Because gabbroic rocks are intrusive and by definition form deeper (≥2 km) within an oceanic crustal column than basaltic volcanics, this source of heterogeneity is likely to be most common in subduction zones where the volcanic and pelagic component of the oceanic crust is relatively thin and trench sediment supply is low, such that slightly deeper sections of the oceanic crust can be incorporated into the subduction interface shear zone. Alternatively, in a hyper-extended margin or magma-poor

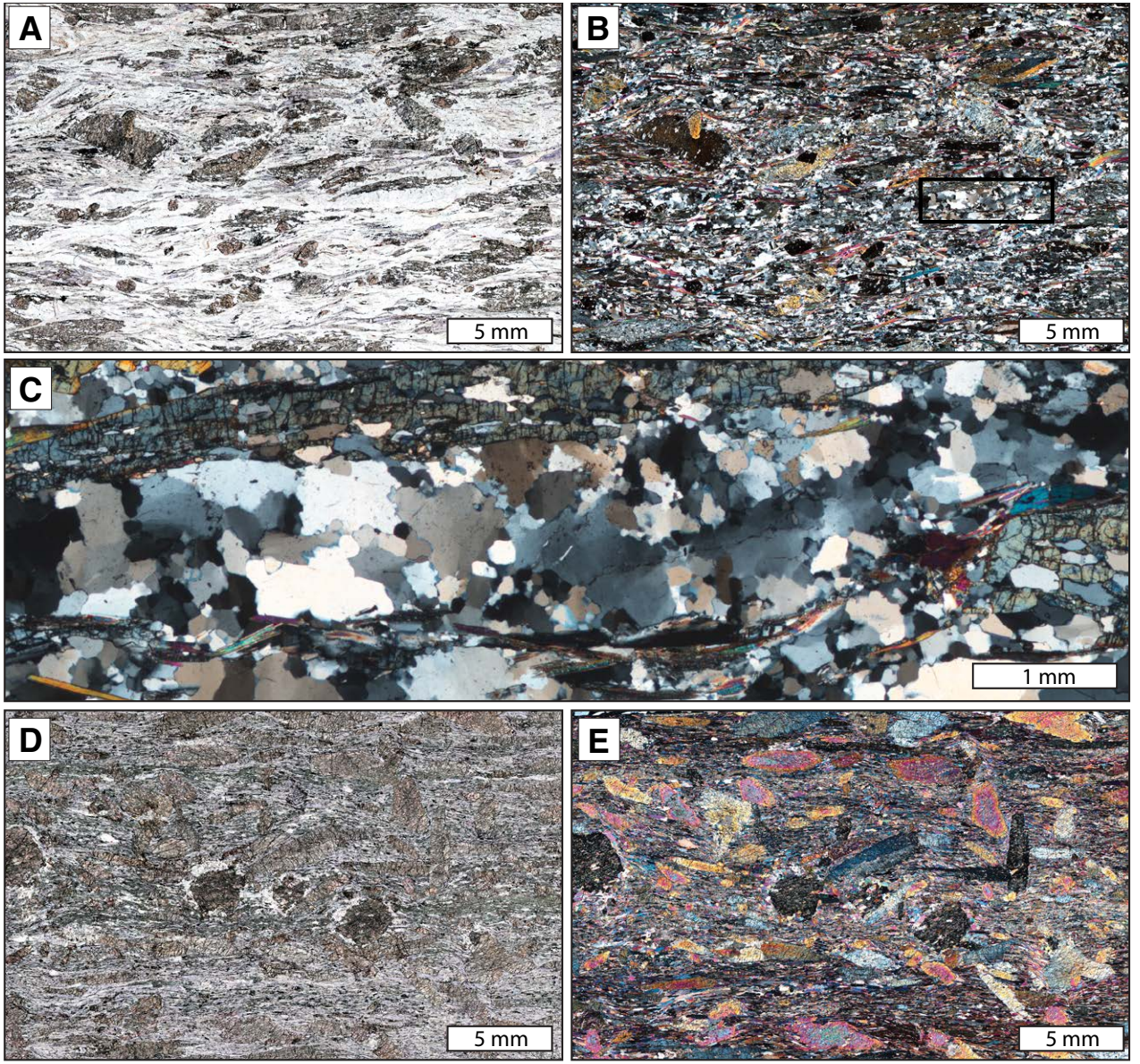

Figure 11. Representative photomicrographs of Fabrikas matrix rock microstructures. (A–C) Garnet-bearing glaucophane-epidote quartz mica schist, plane-polarized light (PPL) (A) and cross-polarized light (XPL) (B, C). Extensional C′-type shear bands are developed throughout. Glaucophane crystals are brittlely boudinaged within the foliation and along C′ cleavages and are partially replaced by green amphibole. Black box in (B) corresponds to area shown in (C). (C) Quartz microstructure with subgrain formation and grain boundary migration. (D, E) Glaucophane-omphacite blueschist matrix containing poikiloblastic garnet and zoned epidote, PPL (D) and XPL (E). Note consistent, fine-grain sizes and consistent extinction behavior of glaucophane and omphacite.

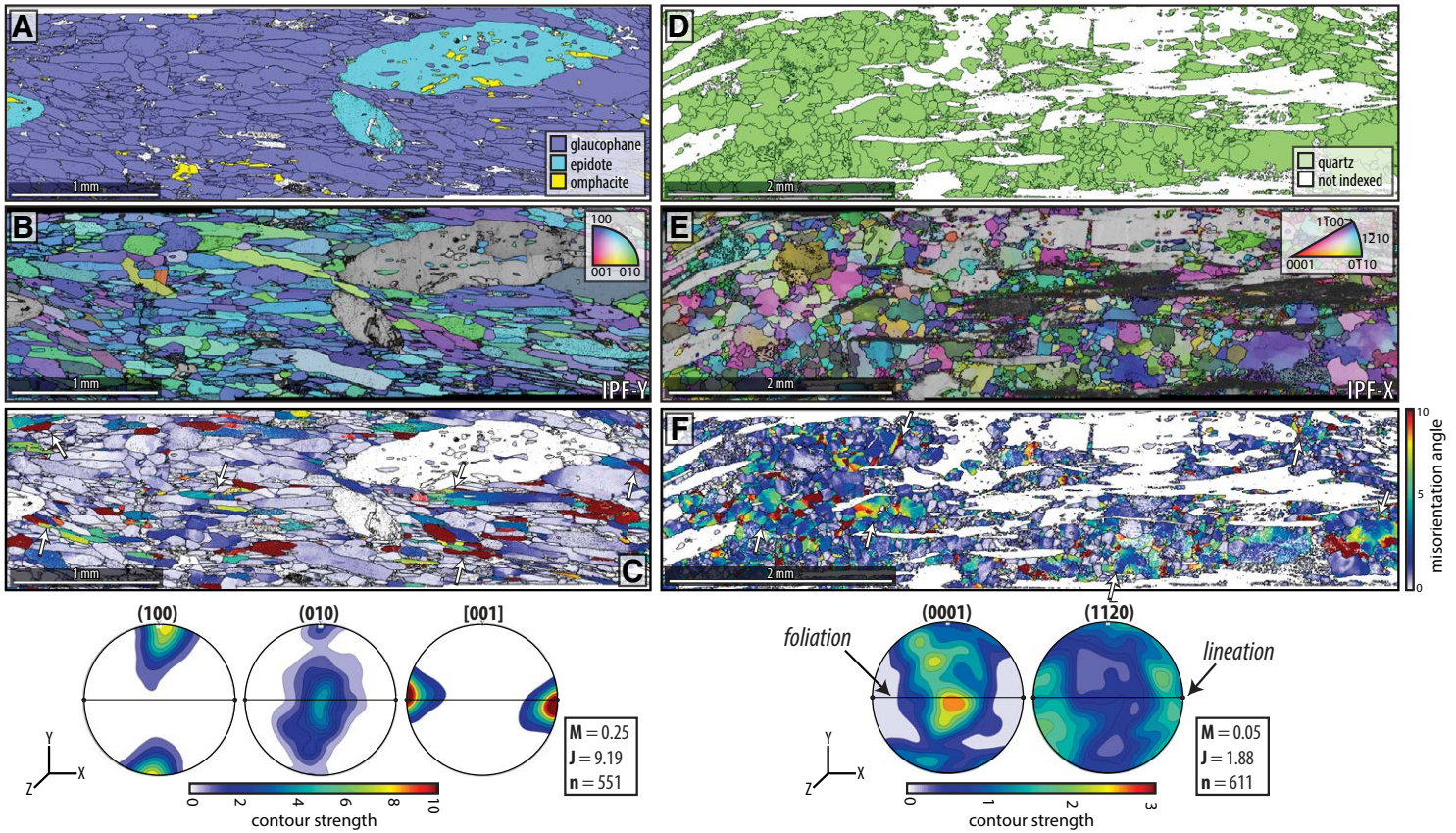

Figure 12. Electron backscatter diffraction (EBSD) maps of blueschist and quartz-mica schist matrix rocks at Fabrikas (left panel is sample KCS66; right panel is sample KCS65). (A, D) Phase maps; (B, E) Inverse pole figure maps (Y-vector for glaucophane, left; X-vector for quartz, right) with inset color-coded keys. Similar blue-purple colors for glaucophane indicate that the (100) crystallographic axes are oriented mostly parallel to the Y-vector in this reference frame (vertical, perpendicular to foliation). Combination of purple-blue-green colors indicates the <a> crystallographic axes are parallel to the X-vector (horizontal, parallel to lineation). See also the pole figures below. (C, F) Misorientation maps showing intracrystalline plastic strain and subgrain formation in glaucophane (left) and quartz (right), with color bar showing degrees of intracrystalline misorientation (°). White arrows point to areas that best highlight subgrain structure and porphyroclasts with surrounding recrystallized grains. Pole figures of lattice-preferred orientations (LPOs) for glaucophane, showing (100) and (010) crystallographic planes and [001] direction, and for quartz, showing <c> and <a> planes, respectively. Pole figures are point per grain. Fabric strengths were calculated using the M and J indices as indicated (Skemer et al., 2005; Bunge, 1982). n—number of grains reported.

rift setting, gabbros may be exposed on the seafloor through exhumation along oceanic core complex detachments (Péron-Pinvidic et al., 2007; Masini et al., 2013). In this scenario, discontinuous igneous pockets are surrounded by exhumed, hydrated subcontinental mantle (Beltrando et al., 2014) (Fig. 13, cross sections). The juxtaposition of different rock types on the seafloor sets up another type of rheological contrast, such that weaker serpentinites may localize strain around stronger gabbro pods during subduction (Fig. 13, insets C and D). Incorporation of gabbros into the subduction shear zone can be achieved, therefore, by detachment of a normal crustal sequence from the subducting plate along a rheologically weak layer such as serpentinite and/or a zone within the lower crust affected by fracturing and alteration prior to subduction, or by subduction of a hyper-extended margin. Alternatively, mafic intrusive igneous rocks can potentially be incorporated into the subduction channel via erosion of the forearc in subduction erosion environments (Cloos and Shreve, 1988; von Huene and Scholl, 1991; Stern, 2011).

The eclogitic lenses in a blueschist matrix at Kini demonstrate that even in a single basaltic protolith, substantial rheological heterogeneity develops as a result of partial dehydration to form eclogite (cf. Behr et al., 2018). Behr

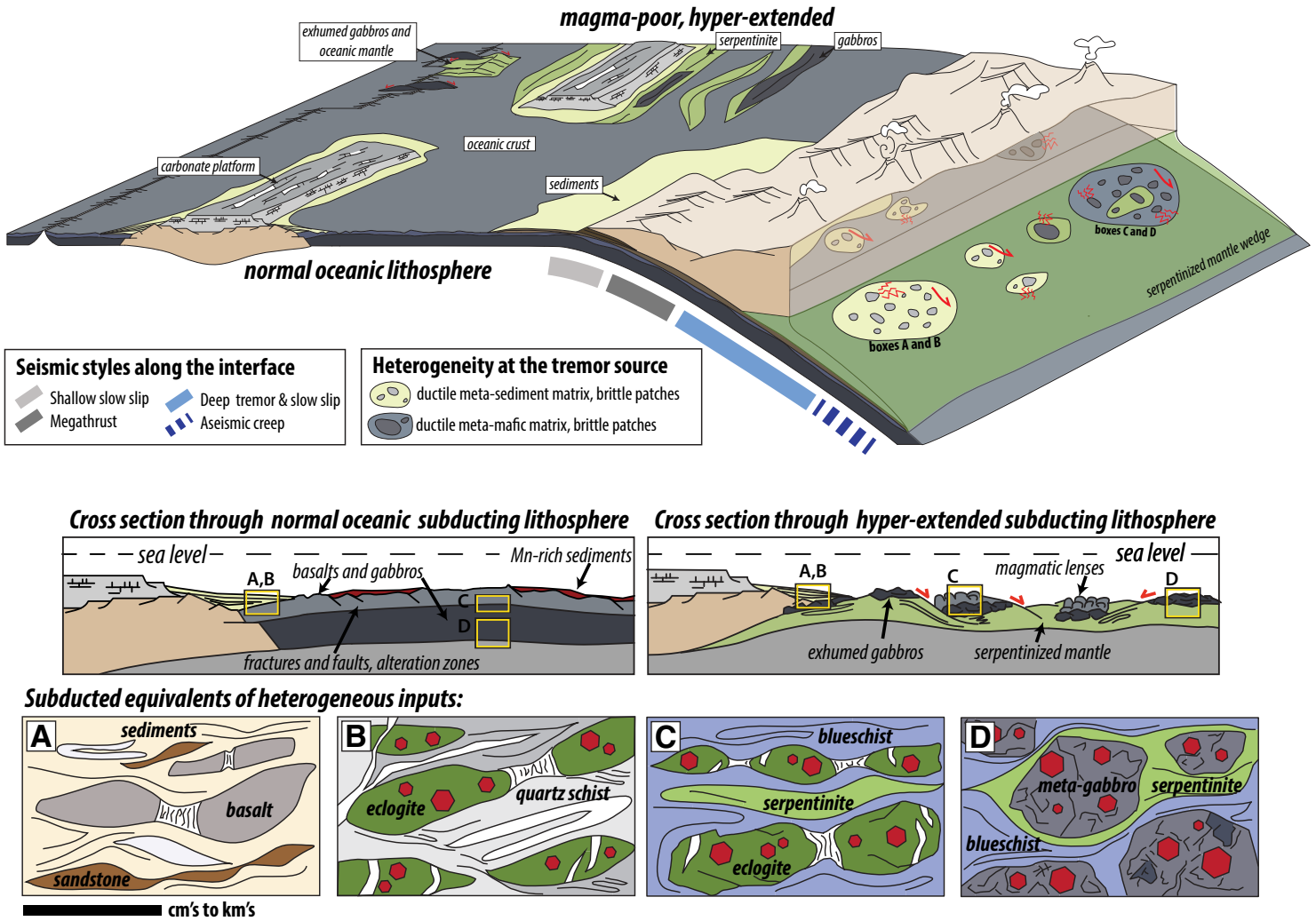

Figure 13. Schematic tectonic setting illustrating potential sources and consequences of heterogeneity entering a subduction zone. Cross sections through magma-poor and magma-rich rifted margins show juxtaposition of different rock types such as sediments, rift volcanics, continental basement, and/or hydrated mantle, which provide sources of primary lithological, geochemical, and textural heterogeneity. Boxes A–D illustrate the fate of different kinds of primary heterogeneity when subducted: (A) Primary lithological heterogeneities lead to competency contrasts between basalts and/or sandstones and sediments along the shallow interface. If subducted to eclogite facies, the lithological heterogeneity in (A) evolves to metamorphic heterogeneity shown in (B) (e.g., Fabrikas). Slight differences in chemistry throughout the upper crust (C) and/or grain size and igneous texture (D) may favor different metamorphic equivalents at high-pressure low-temperature (HP/LT) conditions, such that weaker blueschists and stronger eclogites and/or meta-gabbros coexist under identical pressure-temperature (PT) conditions (e.g., Kini and Agios Dimitrios). The matrix material in (C) and (D) will contain varying proportions of basalt and/or gabbro, serpentinite, and/or chlorite schist depending on the proportion of mafic to ultramafic rocks exposed on the seafloor and incorporated into the interface shear zone. The features shown in boxes A–D are visible on a range of length scales, from sub-centimeters to meters, and sometimes map scale. At episodic tremor and slow slip (ETS) depths, low-frequency earthquakes (LFEs) and tremors are derived from transient brittle shear of rheologically strong sub-patches within weak, ductile patches. ETS events are derived from source areas that can span many square kilometers, and individual LFE families are contained within these patches.

et al. (2018) interpreted the Kini rocks to record deformation at the blueschist-to-eclogite transition, with the transition between the two likely reflecting minor differences in hydrothermal seafloor alteration prior to subduction (e.g., Spandler et al., 2004). More generally, however, several other factors can lead to "patchy" dehydration and/or preferential metamorphism such that the eclogite reaction is incomplete, including differences in (1) basaltic protolith grain size (Hacker, 1996); (2) bulk chemistry or water content due to magmatic differentiation (El-Shazly et al., 1997); and/or (3) fluid persistence due to the presence of an impermeable upper plate (Abers, 2005). This source of rheological heterogeneity is likely to be most common in sediment-poor subduction zones where a chemically and texturally heterogeneous volcanic upper crust becomes incorporated into the subduction interface shear zone (Fig. 13, cross sections).

The mixed-lithology heterogeneities preserved at Fabrikas reflect coeval subduction of sediments and mafic oceanic crust. Interestingly, however, differences in these protoliths do not appear to produce rheological heterogeneity in the viscous regime unless, or until, the mafic rocks are metamorphosed to form eclogite. We reason this to be the case based on the uniform strain exhibited by layered quartzites and mafic blueschist at the outcrop scale at Fabrikas (Fig. 10), which suggests the different rock types have similar viscosities at blueschist-facies conditions. This is in contrast to exhumed shear zones from the shallow subduction interface, where sediments and basaltic lenses show strong rheological contrasts (e.g., Kimura and Mukai, 1991; Meneghini and Moore, 2007; Fagereng and Diener, 2011). Because the Fabrikas locality records stages of exhumation, it also demonstrates the persistence of eclogitized metabasites as rheologically strong features in the subduction channel during retrogression and return flow. The length scales and distributions of these mixed-lithology heterogeneities may vary substantially, however, as a function of: (1) the ratio of subducted sedimentary to mafic rocks; (2) the viscosity of the matrix; and/or (3) the amount of finite strain accumulated (Lloyd and Ferguson, 1981; Jessell et al., 2009; Abe and Urai, 2012; Schmalholz and Maeder, 2012). Eclogite pods contained within metasedimentary matrix rocks have been described for several other HP terranes; their sizes range from tens of centimeters to tens of meters in diameter, similar to the length scales observed on Syros (Lardeaux and Spalla, 1991; Gao et al., 1999; Davis and Whitney, 2008). This type of mixed-lithology heterogeneity is likely quite common in subduction zones, since many show abundant evidence for sediment subduction to the depths of arc magma genesis (Tera et al., 1986; White and Dupré, 1986; Plank and Langmuir, 1993).

4.2 Mechanical Behavior of the Deep Interface

4.2.1 Bulk-Rock Creep Mechanisms and Interface Rheology

Geophysical models describing the mechanical behavior of the deep subduction interface commonly approximate the plate boundary as a planar frictional fault (e.g., Shimamoto, 1986; Shibazaki, 2003; Liu and Liu, 2005; Rubin, 2008). However, the structural and microstructural observations from Syros suggest that the bulk-rock creep mechanism in the subduction shear zone was distributed power-law viscous flow accommodated by dislocation creep in both mafic oceanic-affinity blueschists and quartz-rich metasediments. Evidence for this includes the abundant observations of intracrystalline plasticity, grain boundary migration, dynamic recrystallization, and lattice-preferred orientations discussed in Section 3.

In many other subduction complexes, especially those deformed at lower temperatures, carbonate and quartz-rich metasedimentary rocks preserve evidence for Newtonian viscous creep during subduction accommodated by pressure solution and/or granular flow (Stöckhert et al., 1999; Stöckhert, 2002; Behr and Platt, 2013; Wassmann and Stöckhert, 2013; Fagereng and den Hartog, 2016; Platt et al., 2018). On Syros and farther south in Crete, the preservation of unstrained aragonite pseudomorphs in meta-carbonate packages, well-developed dissolution seams, and strong shape-preferred orientations of calcite-aragonite marbles indicate that pressure solution creep was the dominant deformation mechanism during subduction (Stöckhert et al., 1999). Strong c-axis preferred orientations in aragonite pseudomorphs indicate that at or near peak conditions, marbles entered the dislocation creep deformation regime (e.g., Brady et al., 2004). Similarly, quartz-rich rocks on Syros described here display pressure-solution fabrics that are subsequently overprinted by dislocation creep. Behr and Platt (2013) suggested, based on subduction complex rocks exposed in southern Spain, that as quartz-rich rocks approach peak PT conditions, thermally activated plastic mechanisms may be favored due to an increase in grain size and/or water fugacity. Additionally, as quartz-rich rocks are cycled back to shallower crustal levels during return flow (e.g., as at the Fabrikas locality) higher shear stresses and lower temperatures may favor dislocation creep, while simultaneous partitioning of water into retrogressive minerals may suppress diffusion creep mechanisms such as pressure solution (Behr and Platt, 2013; Xia and Platt, 2017). In contrast to quartz-rich rocks, flow-law parameters for common minerals in blueschists such as glaucophane and epidote are poorly constrained. However, several natural observations, including our data from this study, suggest that power-law viscous creep is a dominant deformation mechanism in blueschists during both subduction and exhumation (Kim et al., 2013; Behr et al., 2018) (Figs. 7 and 12).

Following the interpretation that subduction mechanics are best described by power-law viscous flow, in Figure 14A, we plot viscosity as a function of temperature for a variety of strain-accommodating rock types on Syros using experimentally-derived constitutive flow laws to gain insight into bulk interface rheology. Viscosities are plotted for a strain rate of 10^{-12} s^{-1}, which is generally consistent with a shear zone thickness between ~300 m–3 km and subduction velocities ~1–5 cm/yr. Bulk shear zone rheology, strength, and viscosity will depend on the phases, their relative proportions, and their spatial distributions in the shear zone (Handy, 1990, 1994; Ji, 2004; Beall et al., 2019). Our observations from Syros suggest that two length scales of heterogeneities exist—at the map scale and at the outcrop scale—each defined by

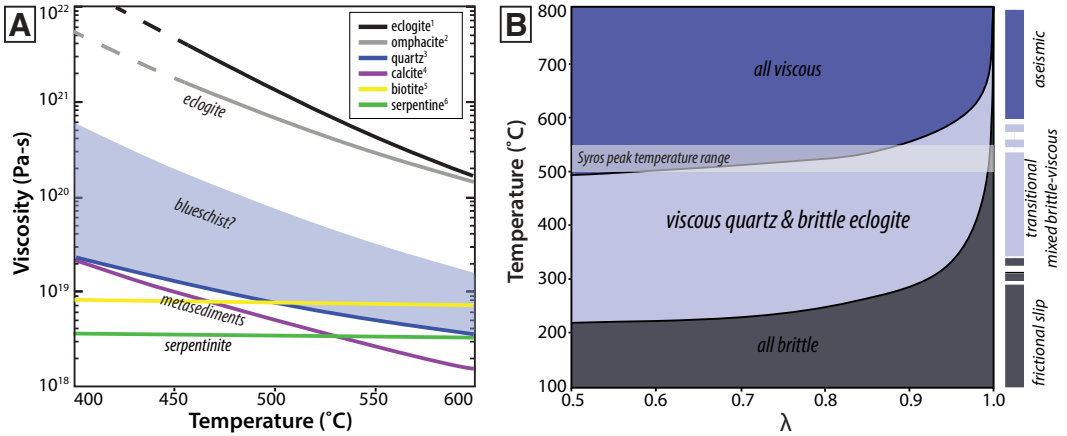

Figure 14. (A) Viscosity as a function of temperature for a variety of rock types common in subduction zones. Viscosities are calculated for a strain rate of 1×10^{-12} s^{-1}. Constitutive equations from: 1—Zhang and Green (2007); 2—Zhang et al. (2006); 3—Hirth et al. (2001); 4—Schmid et al. (1980); 5—Kronenberg et al. (1990); 6—Hilairet et al. (2007). (B) Temperature versus pore fluid pressure factor (λ) deformation mechanism map showing fields where quartz and eclogite are expected to behave by viscous dislocation creep, by brittle failure in eclogite and viscous creep in quartz, and by brittle failure in both rock types. For the maximum temperature range for Syros rocks, eclogites are brittle in the presence of elevated pore fluid pressure (≥0.7).

distinct phase mixtures, proportions, and distributions. Therefore, the "bulk" mechanical behavior of the deep subduction interface should be described as a scale-dependent property.

At the map scale, the juxtaposition of different lithologies leads to rheological heterogeneity that affects bulk rheology. In the uppermost structural unit, slivers of serpentinite and/or chlorite-talc schist several meters to tens of meters thick are located throughout and at the margins of meta-mafic blocks (e.g., Kini and Agios Dimitrios; Fig. 1); in contrast, in the intermediate structural unit, mixed quartz-schist and meta-volcanic exposures (e.g., Fabrikas) are peppered throughout a matrix of marbles and calc-schists (Fig. 1; Keiter et al., 2004, 2011). The spatial associations and relative distributions of rock types are reminiscent of framework-controlled (weak inclusions of serpentinite in a strong matrix of blueschist-eclogite; Fig. 13, box C) and matrix-controlled (strong inclusions of meta-volcanics in a weak matrix of marble; Fig. 13, box B) mixtures, respectively. However, according to phenomenological equations describing the steady-state rheology of two-phase mixtures, bulk shear zone viscosity will rapidly approach that of the volumetrically dominant phase (if the inclusions comprise ~30% by volume or less) (e.g., Handy, 1990, 1994; Ji, 2004).

These inferences are consistent with structural observations in the Syros rocks (cf. Section 3). For example, serpentinites and chlorite and/or talc schists likely did not exert primary control on interface rheology for the uppermost unit. Serpentine has a plastic yield strength and effective viscosity ~1–2 orders of magnitude lower than eclogite (and presumably blueschist) (Fig. 14A) and would preferentially localize strain if possible, yet blueschists accumulated multiple generations of penetrative strain during subduction indicating they were the rheologically dominant phase. Therefore, dislocation creep in framework meta-basalts (e.g., glaucophane) and a viscosity between that of quartz and eclogite (but much closer to quartz, e.g., $8 \times 10^{18} < \eta << 8 \times 10^{20}$ Pa-s at ~500 °C) may best approximate the rheology of subducted oceanic crust under blueschist-facies conditions. Exceptions presumably exist for the extreme circumstance where serpentinite is present in much greater proportions than seen on Syros (e.g., a subducted hyper-extended margin). In contrast, quartz and marble have similar viscosities during subduction to peak conditions (Fig. 14A), and strain would be partitioned locally into both phases. However, the volumetric dominance suggests that dislocation creep in matrix marble may best approximate the bulk rheology and viscosity in the intermediate unit on Syros (approaching ~5×10^{18} Pa-s at ~500 °C).

At the outcrop scale, the juxtaposition of different metamorphic rock types and lithologies produces heterogeneity that will affect bulk rheology. Here, with the goal of a more generalized comparison between Syros and active subduction zones, we envision the three exposures discussed in Section 3 as analogs for subducted oceanic crust (Kini and Agios Dimitrios) and subducted oceanic crust and sediments (Fabrikas) (cf. Section 4.1). At Kini and Agios Dimitrios, eclogite pods distributed in a blueschist matrix are traceable throughout the outcrops (cf. Sections 3.1 and 3.2; Figs. 4 and 8); the proportion of the strong phase (eclogite) is ~1%–10%. At Fabrikas, however, eclogite pods are distributed more densely through a mixed blueschist-quartz schist matrix (cf. Section 3.3; Fig. 10), approaching ~30% on average. A significant proportion (~30% or greater) of strong, competent clasts relative to weak matrix rocks may lead to the development of force chains and clast interactions, effectively amplifying shear stresses, and significantly increasing the bulk shear zone viscosity (e.g., Fagereng and Sibson, 2010; Beall et al., 2019). Stress amplification within "clasts" (eclogites) may lead to the onset of brittle failure in the clasts, even in the absence of elevated pore fluid pressures (Beall et al., 2019). Therefore, concentrations of eclogitic heterogeneities in subducted oceanic crust with or without sediments may approach critical thresholds wherein shear zone jamming and stress amplification occurs across the interface, leading to higher bulk viscosities and perhaps complex transient behavior.

Geodynamic models of subduction dynamics have illustrated the profound effects of non-Newtonian rheology and absolute viscosity on subduction channel morphology, rates and styles of exhumation, and even subduction plate speeds. For example, Gerya et al. (2002) show that non-Newtonian rheologies (and relatively high effective viscosities, ~10^{18} Pa-s) in the channel favor the formation of large-scale, self-organizing, coherent flow patterns, which are reminiscent of nappe structures characteristic of many exhumed subduction terranes, including Syros. Additionally, exhumation by forced return flow in a subduction channel is predicted to occur much faster—on the order of plate velocities—for Newtonian, low-viscosity shear zones (Gerya and Stöckhert, 2002). Furthermore, non-Newtonian, higher-viscosity shear zones are capable of transferring stress from the subducting to the overriding lithosphere more efficiently, leading to greater degrees of mechanical coupling (e.g., Androvičová et al., 2013; Agard et al., 2018) and relatively slow subducting plate speeds (~2–4 cm/yr) compared to a Newtonian, lower-viscosity shear zone (>10 cm/yr) (King and Hager, 1990; Behr and Becker, 2018). In all of these cases, the predominance of dislocation creep in quartz schists and mafic schists is likely to contribute to complex evolution in subduction zone structure and dynamics, as different materials with evolving rheological properties cycle through the subduction shear zone.

In addition to steady-state dynamics and bulk interface viscosity, power-law viscous creep—as opposed to rate-and-state friction along a planar fault—along the subduction interface is important to understanding rock response to transient stress fluctuations, such as intermediate depth earthquakes and ETS, for several reasons. Firstly, power-law creep mechanisms will affect the rates and spatial distributions of host-rock stress loading and postseismic relaxation, owing to their high stress exponents (n = 3–4) (Poirier, 1985; Hirth and Kohlstedt, 2003). Secondly, the mechanisms of "healing," or damage reduction, associated with viscous creep differ from those characteristic of frictional interfaces. For example, damage reduction on faults is achieved by fluid-assisted precipitation of new mineral phases on the fault plane (e.g., Sheldon and Ord, 2005; Sheldon and Micklethwaite, 2007), whereas damage reduction in the viscous regime is commonly achieved by grain growth processes (Handy, 1989; Kameyama et al., 1997). Thirdly, distributed viscous shear in the bulk rock should influence the rates and pathways of fluid migration, through, for example, different diffusion mechanisms and/or through the development of fabric anisotropy (e.g., Kirby, 1985).

4.2.2 Brittle Deformation Associated with Heterogeneities

Independent of the host-rock creep mechanisms, the three exposures on Syros each preserve structural relationships that record multiple generations of dilational, mineralized shear fractures (e.g., "dilational hydro-shears" documented by Fagereng, 2011) in meta-mafic heterogeneities in the presence of fluids. Key lines of evidence for this include crosscutting vein generations filled with a variety of high-pressure minerals. At Kini, for example, glaucophane, phengite, and chlorite occupy veins forming under blueschist-facies conditions. Additionally, vein-filling phengites at Kini have relatively high Si per formula unit values (Behr et al., 2018) that are comparable to those reported for blueschist-facies metamorphism elsewhere in the Cyclades (e.g., Putlitz et al., 2005; Bröcker et al., 2013), which indicate they are growing (and veins are opening) under relatively high pressures consistent with blueschist-facies conditions. Semi-brittle, low-Na omphacite porphyroblasts are fringed by asymmetric pressure shadows with higher-Na omphacite, and Riedel shear fractures are decorated with high-Na omphacite and glaucophane, indicating coupled brittle-viscous shear occurred in Kini blueschists under increasing pressure conditions during subduction (cf. Figs. 6A and 6B). At Agios Dimitrios, the oldest blueschist-facies veins (glaucophane + epidote) are crosscut by younger greenschist-facies veins (actinolite ± epidote), which indicate repeated vein cycles during exhumation (cf. Section 3.2, Fig. 8). At Fabrikas, glaucophane-filled veins indicate eclogites are transiently brittle under retrogressive blueschist-facies conditions (cf. Section 3.3, Fig. 10). At all localities, older generations of veins are commonly rotated into parallelism with the dominant matrix and crosscut by younger, higher-angle veins indicating fracture and vein-fill events occurred in multiple cycles through time (cf. Section 3).

The structural relationships also suggest that transient brittle deformation in meta-mafic heterogeneities is synkinematic with viscous shear in the surrounding host rock. At Kini, for example, evidence for coeval brittle-viscous deformation in eclogitic lenses is documented by brittle shear that decays into viscous shear in surrounding blueschists. Mixed-mode I–III veins open perpendicular to the surrounding blueschist foliation, indicating the fractures are synkinematic with respect to blueschist fabric development. Additionally, foliation-parallel thinning of mineralized boudin necks indicates brittle veining is followed by continuous fabric development in the viscous regime (cf. Figs. 4F and 4G). At Agios Dimitrios, brittle deformation is followed by viscous deformation, as exemplified by some vein sets that are sheared after emplacement (cf. Fig. 8C). At Fabrikas, evidence for coeval brittle-viscous shear is the continuity of high-angle fractures with components of both dilation and shear within eclogite pods and viscous shear bands in the surrounding host rocks (cf. Fig. 10B). At the outcrop scale, the asymmetry of structures in eclogites suggests that they were affected by both viscous (e.g., 10A) and brittle deformation (e.g., Figs. 10B and 10D) during top-to-the-east shearing. Evidence for continuous viscous flow bracketing transient brittle failure is also demonstrated in Figures 4F and 10C, which illustrate several generations of Mode-I veins injected perpendicular to the foliation and progressively transposed parallel to the foliation through time.

The mechanics of this mixed-mode (brittle-ductile and/or frictional-viscous) system can be approximated using experimentally derived constitutive relationships for meta-mafic rocks and metasediments, respectively. In Figure 14B, we plot fields showing deformation modes as a function of temperature and pore fluid factor (ratio of pore fluid pressure to lithostatic pressure, λ) for a quartz-eclogite system deforming by dislocation creep for quartz (Hirth et al., 2001) and eclogite (Zhang and Green, 2007), in a thrust-dominated regime. The plot shows that for the peak temperature conditions on Syros, best represented

by the Kini outcrop, elevated pore fluid factors of >0.7 are required to produce brittle deformation in eclogite. Additionally, the presence of mineralized veins suggests that the pore fluid pressures must be nearly lithostatic, to keep veins and fractures open long enough for fluids to infiltrate and mineralize under extremely high confining pressures. For lower temperatures associated with exhumation of eclogite, as represented by the Agios Dimitrios and Fabrikas outcrops, mixed frictional-viscous deformation of quartz metasediments and persisting eclogites is anticipated for nearly any fluid pressure conditions (except for precisely lithostatic). Thus, this mixed frictional-viscous behavior is predicted for a wide range of conditions within the subduction shear zone, particularly for systems in which mafic eclogites are abundant.

4.3 Compatibility with Episodic Tremor and Slow Slip

To establish whether our observations from Syros may reflect heterogeneous deformation representative of the deep ETS source region, we consider three aspects of ETS as based on modern subduction zones, including: (1) the physical conditions under which tremor occurs, (2) conceptual models for ETS mechanisms, and (3) tremor and LFE source areas and magnitudes.

4.3.1 Physical Conditions

Episodic tremor and slow slip (ETS) appears to occur over a range of PT conditions, most commonly spanning 15–35 km depth within individual subduction zones (Dragert et al., 2001; Obara, 2002; Kao et al., 2005, 2007) but in some places extending as deep as 45–55 km (Kao et al., 2005; Obara and Hirose, 2006; Ito et al., 2007). Geophysical interpretations of the conditions of the ETS source region suggest that tremor and LFE signals are derived from within a low-velocity layer (LVL), or a zone with seismically high Vp/Vs, interpreted as hydrated meta-stable oceanic crust and/or the presence of fluids (Shelly et al., 2006; Wang et al., 2006; Abers et al., 2009; Bostock et al., 2012). Large uncertainties in LFE relocations produce wide apparent vertical distributions of seismic tremors throughout the forearc crust and might suggest tremor does not occur exclusively along the down-going subducting slab, but also within the overriding plate (e.g., Kao et al., 2005, 2007; Peterson and Christensen, 2009). Furthermore, ETS is sensitive to external tidal forces, suggesting the system is critically stressed and under high pore fluid pressures (Rubinstein et al., 2008), and P-wave first arrivals demonstrate that most tremor involves shear slip at or near the plate interface (Obara 2002; Rogers and Dragert, 2003; Dragert et al., 2004; Ide et al., 2007; Shelly et al., 2007a).

Our observations from Syros are consistent with these interpretations. The three different outcrops on Syros demonstrate that rheological heterogeneities exist over a range of PT conditions and protolith rock types. We interpret the strong heterogeneities (eclogites and metagabbros) to have formed within a subduction channel during subduction to eclogite-facies depths (e.g., Kini); we suggest they then persisted as heterogeneities during exhumation along the interface under blueschist- to greenschist-facies conditions (e.g., Fabrikas and Agios Dimitrios outcrops). The discrepancies in reported peak pressure estimates for Syros correspond to a wide range in potential subduction depths. Maximum pressures of 14–16 kbar correspond to ~45–55 km, whereas pressures of ~22–23 kbar correspond to ~75–80 km depth. The former would place these rocks just downdip of the typical ETS zone (~15–35 km), while the latter is >30 km in excess. However, regardless of the peak pressures and maximum depths these rocks reached, the rheological heterogeneities and structural features we report here were acquired during subduction to peak depths (e.g., Kini), and in some cases were continuously modified during exhumation (e.g., Fabrikas and Agios Dimitrios). Therefore, we suggest that eclogites may be capable of contributing to ETS as they pass through typical "tremorgenic" depths during both subduction and exhumation within a subduction channel along the top of the slab. Additionally, the rocks represent partially hydrated oceanic crust and sediments that have retained hydrous phases to ~50–80 km depth, consistent with characteristics of the LVL. Finally, as discussed in Section 4.2, the deformational style in the heterogeneous lenses is consistent with brittle shear slip under high pore fluid pressures in the presence of fluids.

4.3.2 Conceptual Models for ETS Mechanisms

A common conceptual model for the production and repetition of LFEs and tremor is coseismic failure of small interface patches contained within a larger shear zone patch that otherwise creeps aseismically (e.g., Shelly et al., 2007a; Fagereng and Sibson, 2010; Beeler et al., 2014; Hayman and Lavier, 2014; Chestler and Creager, 2017b). These patches, or "asperities," fall into two end-member categories invoking the theme of heterogeneity. The first involves contrasts in frictional properties, wherein conditionally velocity-weakening patches are surrounded by velocity-strengthening areas along a planar interface (Ito et al., 2007; Ando et al., 2012; Ghosh et al., 2012). This model is supported by friction experiments and rate-and-state–dependent friction laws (Shimamoto, 1986; Liu and Rice, 2005, 2007; Shibazaki and Shimamoto, 2007; Rubin, 2008). The second model, derived from geologic observations of exhumed shear zones, involves brittle-viscous heterogeneities in distributed shear zones with competency contrasts reflecting mixed protoliths (Fagereng and Sibson, 2010; Hayman and Lavier, 2014; Malatesta et al., 2018). High pore fluid pressures and low effective stress due to metamorphic dehydration are a likely cause of co-seismic brittle failure, corroborated by dehydration experiments on high-pressure minerals producing low-frequency seismic emissions (Burlini et al., 2009). Some specific proposed evidence for ETS in the rock record includes dilational microcracking and healing by quartz precipitation accompanied by shear slip on micaceous cleavage planes (Platt et al., 2018), mutually crosscutting foliation-parallel and foliation-oblique, quartz-filled veins that accommodate both shear and dilation (Fagereng, 2011; Fagereng et al., 2014, 2017), and mixed-mode dilational-shear fractures that offset competent

lenses within dynamically recrystallized matrices (Hayman and Lavier, 2014). All of these potential records of tremor and slow slip are alike in that they preserve localized, transient (semi-) brittle deformation assisted by fluids, coeval with viscous flow, from submillimeter to outcrop scales.

These conceptual models are also consistent with the observation that LFE families have exponential moment-frequency distributions (Watanabe et al., 2007; Shelly and Hardebeck, 2010; Sweet et al., 2014) and characteristic seismic moments (Chestler and Creager, 2017b), implying that there is a scale-limited process occurring at the tremor source (Bostock et al., 2015; Chestler and Creager, 2017b). Given that seismic moment is defined as:

$$M_0 = \mu AD, \quad (1)$$

where μ is rock rigidity, A is the source area, and D is the displacement magnitude, the observed characteristic seismic moments could be limited by the amount of slip displacement during an event, or the area that slips during an event, or both. Observations of weak positive scaling between LFE moment and duration (Bostock et al., 2015; Thomas et al., 2016) and wide ranges in geodetically determined slip magnitudes from <1 mm to 6 cm among ETS events and LFE families (Szeliga et al., 2008; Sweet et al., 2014; Chestler and Creager, 2017a) favor an area-limited, rather than displacement-limited source process. An area-limited process is also consistent with studies that relate the spatial distribution of LFEs, tremor, and slow slip to locations of geologic terranes, tectonic sutures in the upper plate, and/or incoming plate heterogeneity (e.g., Brudzinski and Allen, 2007; Schmidt and Gao, 2010; Li et al., 2018).

Our observations of heterogeneities on Syros are consistent with the brittle-viscous model and also support the area-limited seismic moment concept: the map areas of individual mafic units on Syros can be interpreted as former interface shear zone patches (see for example the mapped lenses for Kini, Agios Dimitrios, and Fabrikas in Fig. 1). Within each mapped patch, there are brittlely deformed heterogeneities (eclogite and meta-gabbro lenses) that could potentially represent tremor-producing sub-patches (Fig. 13). According to the conceptual model described above, the remainder of the geodetically observed slip on the surface would be accommodated by accelerated viscous creep in surrounding blueschist and quartz schist matrix rocks.

4.3.2 Seismic Moment and Tremor Magnitude Estimates

Seismic moment (as defined above) can be converted to moment magnitude through the following relationship:

$$M_w = \frac{2}{3} \log_{10}(M_0) - 10.7 \quad (2)$$

(Kanamori, 1977). We can use this relationship and our observations from Syros to estimate the maximum moment magnitudes that would be expected from the interface patches analyzed at Kini, Agios Dimitrios, and Fabrikas, if they were capable of producing tremor. These calculations require the following assumptions.

1. The present-day map patterns of different rock types on Syros approximate the length scales of heterogeneous patches within the interface shear zone during subduction, and the percentages of heterogeneities observed in subregion exposures are characteristic of the entire shear zone patch. Our field observations suggest that the types and distributions of documented heterogeneities are characteristic of the map areas shown in Figure 1. This allows us to estimate source area (A) by multiplying the mapped area of the lithological unit represented by the outcrop (cf. Fig. 1) by the ratio of brittle heterogeneities documented for a subregion within that outcrop (cf. Supplemental Fig. S1 and Table S4 [footnote 1]).
2. Brittle shear slip of mafic lenses within these interface shear zone patches occurred simultaneously or within close succession. Although we cannot confirm that this was the case through field observations, it is not an unreasonable assumption because there are several mechanisms by which shear zone deformation can propagate transiently within a viscous interface shear zone, including via the generation of porosity waves (e.g., Skarbek and Rempel, 2016), the development of stress bridges among competent clasts (e.g., Webber et al., 2018; Beall et al., 2019), or viscoelastic interactions among clasts. Furthermore, this assumption is also compatible with observations of modern tremor bursts, which consist of swarms of small, low-frequency earthquakes rather than single events (Ito et al., 2007; Shelly et al., 2007b). The assumption of simultaneous failure then allows us to equate our observed displacement amounts on individual brittle lenses to total displacement over the whole interface area, A, discussed above. This assumption also means that our moment magnitude estimates are maximums.
3. For rock rigidity, we assume 30–40 GPa for oceanic crust at eclogite-facies depths; as reasoned by Sweet et al. (2014), 30 GPa splits the difference between normal oceanic crust at these depths (40 GPa) and values for highly anomalous upper oceanic crust with Vp/Vs ratios ~2.4 (Audet et al., 2009).

Additional details about these calculations and how uncertainties were treated are presented in the Supplemental Text (footnote 1).

Figure 15 compares our calculations of source area and observed displacement to those estimated from tremor-producing regions in active subduction zones. The gray data points in Figure 15 include LFE source areas estimated using high-resolution spatial relocation of LFE events, and displacement magnitudes calculated through inversion of the seismic moment equation, where seismic moments were estimated by stacking LFE events and comparing their amplitudes with local small earthquakes of known magnitudes (Kao et al., 2010; Sweet et al., 2014; Bostock et al., 2015; Thomas et al., 2016; Chestler and Creager, 2017b). Our displacements in Figure 15 are limited by the smallest size of documented eclogite pods and lenses for each locality. We provide equivalent circle diameters (ECDs) of calculated map and source areas in Table S5 (footnote 1) to compare with similar measurements derived from geophysical

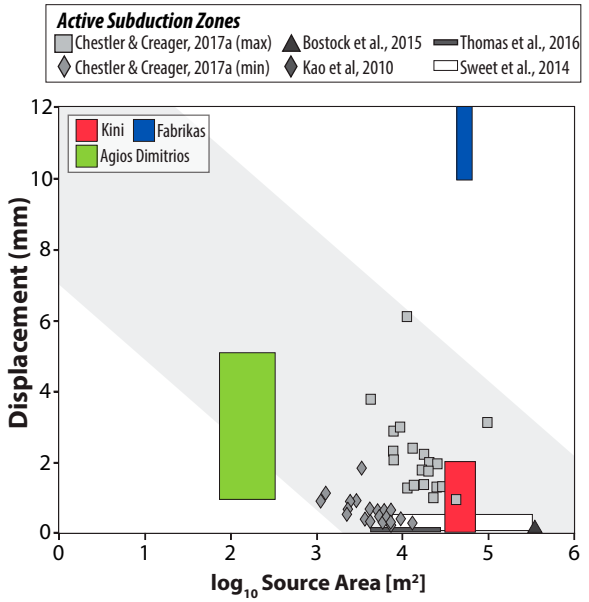

Figure 15. Observed low-frequency earthquake (LFE) source areas and calculated tremor-genic coseismic displacement from active subduction zones in gray symbols from Sweet et al. (2014), Chestler and Creager (2017a), and Bostock et al. (2015), with the general trend between the two outlined in the gray bar. Colored boxes are estimated source areas and ranges of coseismic displacement limited by the smallest asperity size from the three localities on Syros, determined from field and microstructural observations. See Supplemental Material (text footnote 1) for tables of source areas, offset measurements, and magnitude calculations.

data; our patch and source area ECDs range from ~400 to 1000 m and ~10 to 300 m, respectively, the same order of magnitude as areas calculated by Chestler and Creager (2017a), Sweet et al. (2014), and Thomas et al. (2016). Both the Kini and Agios Dimitrios localities have displacement versus source area scaling that is consistent with observations from Cascadia. The Fabrikas locality is inconsistent, perhaps suggesting that heterogeneities there record the superposition of smaller slip events. Our calculations from Syros suggest that the simultaneous or successive brittle failure of heterogeneous lenses with the documented length scales could yield equivalent seismic moments of 4.5×10^9 to 4.6×10^{14} N m (Mw ~0.3–3.7), entirely compatible with observed seismic signals in the ETS source region (Fig. 14B).

5. CONCLUSIONS

Exhumed rocks on Syros Island provide insight into the mechanical behavior of a heterogeneous subduction interface shear zone. Rheological heterogeneities associated with lithological and/or textural differences in the subducting protoliths persist to peak depths and during viscous return flow, are accentuated by eclogite-facies metamorphism, and produce cyclical brittle deformation events triggered by high pore fluid pressures. Brittle deformation is accompanied by viscous power-law flow in surrounding quartz-schist and blueschist host rocks. The Syros rocks exhibit several similarities with the physical conditions of episodic tremor and slow slip in active subduction zones as inferred from geophysical studies—namely: (1) fluid-assisted brittle shear slip in a variety of hydrous rock types over a wide range of PT conditions; and (2) tremor source areas and equivalent seismic moments. Our observations support a conceptual model of tremor-genesis in which coseismic failure occurs in small sub-patches distributed within a larger, viscously creeping interface patch.

ACKNOWLEDGMENTS

This work was supported by a National Science Foundation (NSF) Graduate Research Fellowship awarded to A.J. Kotowski and an NSF CAREER grant (EAR-1555346) awarded to W.M. Behr. Thanks to James Maner for help with the microprobe and environmental scanning electron microscope at University of Texas at Austin. We are grateful to Danny Stockli, Kostis Soukis, Jaime Barnes, Mark Cloos, Luc Lavier, and Laura Wallace for discussions and to four anonymous reviewers for constructive comments that improved this manuscript.

REFERENCES CITED

Abe, S., and Urai, J.L., 2012, Discrete element modeling of boudinage: Insights on rock rheology, matrix flow, and evolution of geometry: Journal of Geophysical Research. Solid Earth, v. 117, B01407, https://doi.org/10.1029/2011JB008555.

Abers, G.A., 1992, Relationship between shallow- and intermediate-depth seismicity in the Eastern Aleutian Subduction Zone: Geophysical Research Letters, v. 19, no. 20, p. 2019–2022, https://doi.org/10.1029/92GL02060.

Abers, G.A., 2005, Seismic low-velocity layer at the top of subducting slabs: Observations, predictions, and systematics: Physics of the Earth and Planetary Interiors, v. 149, no. 1–2, p. 7–29.

Abers, G.A., MacKenzie, L.S., Rondenay, S., Zhang, Z., Wech, A.G., and Creager, K.C., 2009, Imaging the source region of Cascadia tremor and intermediate-depth earthquakes: Geology, v. 37, no. 12, p. 1119–1122, https://doi.org/10.1130/G30143A.1.

Agard, P., Plunder, A., Angiboust, S., Bonnet, G., and Ruh, J., 2018, The subduction plate interface: Rock record and mechanical coupling (from long to short time scales): Lithos, v. 320-321, p. 537–566, https://doi.org/10.1016/j.lithos.2018.09.029.

Ando, R., Takeda, N., and Yamashita, T., 2012, Propagation dynamics of seismic and aseismic slip governed by fault heterogeneity and Newtonian rheology: Journal of Geophysical Research. Solid Earth, v. 117, no. B11, https://doi.org/10.1029/2012JB009532.

Andriessen, P.A.M., Boelrijk, N.A.I.M., Hebeda, E.H., Priem, H.N.A., Verdurnen, E.A.T., and Verschure, R.H., 1979, Dating the events of metamorphism and granitic magmatism in the Alpine orogen of Naxos (Cyclades, Greece): Contributions to Mineralogy and Petrology, v. 69, no. 3, p. 215–225, https://doi.org/10.1007/BF00372323.

Androvičová, A., Čížková, H., and van den Berg, A., 2013, The effects of rheological decoupling on slab deformation in the Earth's upper mantle: Studia Geophysica et Geodaetica, v. 57, no. 3, p. 460–481, https://doi.org/10.1007/s11200-012-0259-7.

Angiboust, S., Agard, P., Raimbourg, H., Yamato, P., and Huet, B., 2011, Subduction interface processes recorded by eclogite-facies shear zones (Monviso, W. Alps): Lithos, v. 127, no. 1–2, p. 222–238, https://doi.org/10.1016/j.lithos.2011.09.004.

Audet, P., Bostock, M.G., Christensen, N.I., and Peacock, S.M., 2009, Seismic evidence for overpressured subducted oceanic crust and megathrust fault sealing: Nature, v. 457, no. 7225, p. 76–78, https://doi.org/10.1038/nature07650.

Avigad, D., and Garfunkel, Z., 1991, Uplift and exhumation of high-pressure metamorphic terrains: the example of the Cycladic blueschist belt (Aegean Sea): Tectonophysics, v. 188, p. 357–372, https://doi.org/10.1016/0040-1951(91)90464-4.

Avigad, D., Garfunkel, Z., Jolivet, L., and Azañón, J.M., 1997, Back arc extension and denudation of Mediterranean eclogites: Tectonics, v. 16, no. 6, p. 924–941, https://doi.org/10.1029/97TC02003.

Bach, W., Alt, J.C., Niu, Y., Humphris, S.E., Erzinger, J., and Dick, H.J., 2001, The geochemical consequences of late-stage low-grade alteration of lower ocean crust at the SW Indian Ridge: Results from ODP Hole 735B (Leg 176): Geochimica et Cosmochimica Acta, v. 65, no. 19, p. 3267–3287, https://doi.org/10.1016/S0016-7037(01)00677-9.

Bach, W., Bernhard, P.E., Hart, S.R., and Blusztajn, J.S., 2003, Geochemistry of hydrothermally altered oceanic crust: DSDP/ODP Hole 504B-Implications for seawater-crust exchange budgets and Sr- and Pb-isotopic evolution of the mantle: Geochemistry, Geophysics, Geosystems, v. 4, no. 3, https://doi.org/10.1029/2002GC000419.

Beall, A., Fagereng, Å., and Ellis, S., 2019, Strength of strained two-phase mixtures: Application to rapid creep and stress amplification in subduction zone mélange: Geophysical Research Letters, https://doi.org/10.1029/2018GL081252.

Beeler, N.M., Thomas, A., Bürgmann, R., and Shelly, D., 2014, Inferring fault rheology from low-frequency earthquakes on the San Andreas: Journal of Geophysical Research. Solid Earth, v. 118, p. 5976–5990, https://doi.org/10.1002/2013JB010118.

Behr, W.M., and Becker, T.W., 2018, Sediment control on subduction plate speeds: Earth and Planetary Science Letters, v. 502, p. 166–173, https://doi.org/10.1016/j.epsl.2018.08.057.

Behr, W.M., and Platt, J.P., 2013, Rheological evolution of a Mediterranean subduction complex: Journal of Structural Geology, v. 54, p. 136–155, https://doi.org/10.1016/j.jsg.2013.07.012.

Behr, W.M., Kotowski, A.J., and Ashley, K.T., 2018, Dehydration-induced rheological heterogeneity and the deep tremor source in warm subduction zones: Geology, https://doi.org/10.1130/G40105.1.

Beltrando, M., Manatschal, G., Mohn, G., Dal Piaz, G.V., Brovarone, A.V., and Masini, E., 2014, Recognizing remnants of magma-poor rifted margins in high-pressure orogenic belts: The alpine case study: Earth-Science Reviews, v. 131, p. 88–115, https://doi.org/10.1016/j.earscirev.2014.01.001.

Beroza, G.C., and Ide, S., 2011, Slow earthquakes and nonvolcanic tremor: Annual Review of Earth and Planetary Sciences, v. 39, p. 271–296, https://doi.org/10.1146/annurev-earth-040809-152531.

Bond, C.E., Butler, R.W.H., and Dixon, J.E., 2007, Co-axial horizontal stretching within extending orogens: The exhumation of HP rocks on Syros (Cyclades) revisited: Geological Society of London Special Publication 272, no. 1, p. 203–222, https://doi.org/10.1144/GSL.SP.2007.272.01.12.

Bonneau, M., 1984, Correlation of the Hellenide nappes in the south-east Aegean and their tectonic reconstruction: Geological Society of London Special Publication 17, no. 1, p. 517–527, https://doi.org/10.1144/GSL.SP.1984.017.01.38.

Bostock, M.G., Royer, A.A., Hearn, E.H., and Peacock, S.M., 2012, Low frequency earthquakes below southern Vancouver Island: Geochemistry, Geophysics, Geosystems, v. 13, no. 11, https://doi.org/10.1029/2012GC004391.

Bostock, M.G., Thomas, A.M., Savard, G., Chuang, L., and Rubin, A.M., 2015, Magnitudes and moment-duration scaling of low-frequency earthquakes beneath southern Vancouver Island: Journal of Geophysical Research, B, Solid Earth, v. 120, no. 9, p. 6329–6350, https://doi.org/10.1002/2015JB012195.

Brady, J.B., Markley, M.J., Schumacher, J.C., Cheney, J.T., and Bianciardi, G.A., 2004, Aragonite pseudomorphs in high-pressure marbles of Syros, Greece: Journal of Structural Geology, v. 26, no. 1, p. 3–9, https://doi.org/10.1016/S0191-8141(03)00099-3.

Bröcker, M., and Pidgeon, R.T., 2007, Protolith ages of meta-igneous and metatuffaceous rocks from the cycladic blueschist unit, Greece: Results of a reconnaissance U-Pb zircon study: The Journal of Geology, v. 115, no. 1, p. 83–98, https://doi.org/10.1086/509269.

Bröcker, M., Baldwin, S., and Arkudas, R., 2013, The geological significance of $^{40}Ar/^{39}Ar$ and Rb-Sr white mica ages from Syros and Sifnos, Greece: A record of continuous (re)crystallization during exhumation?: Journal of Metamorphic Geology, v. 31, no. 6, p. 629–646, https://doi.org/10.1111/jmg.12037.

Brudzinski, M.R., and Allen, R.M., 2007, Segmentation in episodic tremor and slip all along Cascadia: Geology, v. 35, no. 10, p. 907–910, https://doi.org/10.1130/G23740A.1.

Bulle, F., Bröcker, M., Gärtner, C., and Keasling, A., 2010, Geochemistry and geochronology of HP mélanges from Tinos and Andros, cycladic blueschist belt, Greece: Lithos, v. 117, no. 1–4, p. 61–81, https://doi.org/10.1016/j.lithos.2010.02.004.

Bunge, H.-J., 1982, Texture Analysis in Materials Science: Mathematical Methods: London, Butterworths, 614 p., https://doi.org/10.1016/C2013-0-11769-2.

Burlini, L., Di Toro, G., and Meredith, P., 2009, Seismic tremor in subduction zones: Rock physics evidence: Geophysical Research Letters, v. 36, no. 8, https://doi.org/10.1029/2009GL037735.

Byrne, D.E., Davis, D.M., and Sykes, L.R., 1988, Loci and maximum size of thrust earthquakes and the mechanics of the shallow region of subduction zones: Tectonics, v. 7, no. 4, p. 833–857, https://doi.org/10.1029/TC007i004p00833.

Chapman, J.S., and Melbourne, T.I., 2009, Future Cascadia megathrust rupture delineated by episodic tremor and slip: Geophysical Research Letters, v. 36, no. 22, https://doi.org/10.1029/2009GL040465.

Chestler, S.R., and Creager, K.C., 2017a, A Model for Low-Frequency Earthquake Slip: Geochemistry, Geophysics, Geosystems, v. 18, no. 12, p. 4690–4708, https://doi.org/10.1002/2017GC007253.

Chestler, S.R., and Creager, K.C., 2017b, Evidence for a scale-limited low-frequency earthquake source process: Journal of Geophysical Research. Solid Earth, v. 122, no. 4, p. 3099–3114, https://doi.org/10.1002/2016JB013717.

Cliff, R.A., Bond, C.E., Butler, R.W.H., and Dixon, J.E., 2017, Geochronological challenges posed by continuously developing tectonometamorphic systems: Insights from Rb-Sr mica ages from the Cycladic Blueschist Belt, Syros (Greece): Journal of Metamorphic Geology, v. 35, no. 2, p. 197–211, https://doi.org/10.1111/jmg.12228.

Cloos, M., 1992, Thrust-type subduction-zone earthquakes and seamount asperities: A physical model for seismic rupture: Geology, v. 20, no. 7, p. 601–604, https://doi.org/10.1130/0091-7613(1992)020<0601:TTSZEA>2.3.CO;2.

Cloos, M., and Shreve, R.L., 1988, Subduction-channel model of prism accretion, mélange formation, sediment subduction, and subduction erosion at convergent plate margins: 1. Background and description: Pure and Applied Geophysics, v. 128, no. 3, p. 455–500, https://doi.org/10.1007/BF00874548.

Cooperdock, E.H., Raia, N.H., Barnes, J.D., Stockli, D.F., and Schwarzenbach, E.M., 2018, Tectonic origin of serpentinites on Syros, Greece: Geochemical signatures of abyssal origin preserved in a HP/LT subduction complex: Lithos, v. 296, p. 352–364, https://doi.org/10.1016/j.lithos.2017.10.020.

Davis, P.B., and Whitney, D.L., 2008, Petrogenesis and structural petrology of high-pressure metabasalt pods, Sivrihisar, Turkey: Contributions to Mineralogy and Petrology, v. 156, no. 2, p. 217–241, https://doi.org/10.1007/s00410-008-0282-4.

Dixon, J.E., 1976, Glaucophane schists of Syros, Greece: Bulletin de la Société Géologique de France, v. 7, no. 2, p. 280, https://doi.org/10.2113/gssgfbull.S7-XVIII.2.280.

Dixon, T.H., Jiang, Y., Malservisi, R., McCaffrey, R., Voss, N., Protti, M., and Gonzalez, V., 2014, Earthquake and tsunami forecasts: Relation of slow slip events to subsequent earthquake rupture: Proceedings of the National Academy of Sciences of the United States of America, v. 111, no. 48, p. 17,039–17,044, https://doi.org/10.1073/pnas.1412299111.

Douglas, A., Beavan, J., Wallace, L., and Townend, J., 2005, Slow slip on the northern Hikurangi subduction interface, New Zealand: Geophysical Research Letters, v. 32, no. 16, p. 1–4, https://doi.org/10.1029/2005GL023607.

Dragert, H., Wang, K., and James, T.S., 2001, A silent slip event on the deeper Cascadia subduction interface: Science, v. 292, no. 5521, p. 1525–1528, https://doi.org/10.1126/science.1060152.

Dragert, H., Wang, K., and Rogers, G., 2004, Geodetic and seismic signatures of episodic tremor and slip in the northern Cascadia subduction zone: Earth, Planets, and Space, v. 56, no. 12, p. 1143–1150, https://doi.org/10.1186/BF03353333.

El-Shazly, A.K., Worthing, M.A., and Liou, J.G., 1997, Interlayered eclogites, blueschists and epidote amphibolites from NE Oman: A record of protolith compositional control and limited fluid infiltration: Journal of Petrology, v. 38, no. 11, p. 1461–1487, https://doi.org/10.1093/petroj/38.11.1461.

Evans, B.W., 1990, Phase relations of epidote-blueschists: Lithos, v. 25, p. 3–23, https://doi.org/10.1016/0024-4937(90)90003-J.

Fagereng, Å., 2011, Geology of the seismogenic subduction thrust interface, *in* Fagereng, Å., Toy, V.G., and Rowland, J.V., eds., Geology of the Earthquake Source: A Volume in Honour of Rick Sibson: Geological Society of London Special Publication 359, no. 1, p. 55–76.

Fagereng, Å., and den Hartog, S.A.M., 2016, Subduction megathrust creep governed by pressure solution and frictional-viscous flow: Nature Geoscience, v. 10, no. 1, p. 51–57, https://doi.org/10.1038/ngeo2857.

Fagereng, Å., and Diener, J.F.A., 2011, San Andreas Fault tremor and retrograde metamorphism: Geophysical Research Letters, v. 38, no. 23, https://doi.org/10.1029/2011GL049550.

Fagereng, Å., and Sibson, R.H., 2010, Mélange rheology and seismic style: Geology, v. 38, no. 8, p. 751–754, https://doi.org/10.1130/G30868.1.

Fagereng, Å., Hillary, G.W., and Diener, J.F., 2014, Brittle-viscous deformation, slow slip, and tremor: Geophysical Research Letters, v. 41, no. 12, p. 4159–4167, https://doi.org/10.1002/2014GL060433.

Fagereng, Å., Diener, J.F., Meneghini, F., Harris, C., and Kvadsheim, A., 2017, Quartz vein formation by local dehydration embrittlement along the deep, tremorgenic subduction thrust interface: Geology, v. 46, no. 1, p. 67–70, https://doi.org/10.1130/G39649.1.

Forster, M.A., and Lister, G.S., 1999, Detachment faults in the Aegean core complex of Ios, Cyclades, Greece, *in* Ring, U., Brandon, M.T., Lister, G.S., and Willett, S.D., eds., Exhumation Processes: Normal Faulting, Ductile Flow and Erosion: Geological Society of London Special Publication 154, no. 1, p. 305–323.

Fountain, D.M., and Salisbury, M., 1981, Exposed cross-sections through the continental crust: Implications for crustal structure, petrology: Earth and Planetary Science Letters, https://doi.org/10.1016/0012-821X(81)90133-3.

Gao, J., Klemd, R., Zhang, L., Wang, Z., and Xiao, X., 1999, P-T path of high-pressure/low-temperature rocks and tectonic implications in the western Tianshan Mountains, NW China: Journal of Metamorphic Geology, v. 17, no. 6, p. 621–636, https://doi.org/10.1046/j.1525-1314.1999.00219.x.

Gautier, P., and Brun, J.P., 1994, Crustal-scale geometry and kinematics of late-orogenic extension in the central Aegean (Cyclades and Ewia Island): Tectonophysics, v. 238, no. 1–4, p. 399–424, https://doi.org/10.1016/0040-1951(94)90066-3.

Gerya, T.V., and Stöckhert, B., 2002, Exhumation rates of high pressure metamorphic rocks in subduction channels: the effect of rheology: Geophysical Research Letters, v. 29, no. 8, p. 102-1–102-4, https://doi.org/10.1029/2001GL014307.

Gerya, T.V., Stöckhert, B., and Perchuk, A.L., 2002, Exhumation of high-pressure metamorphic rocks in a subduction channel: A numerical simulation: Tectonics, v. 21, no. 6, p. 6-1–6-19, https://doi.org/10.1029/2002TC001406.

Ghosh, A., Vidale, J.E., and Creager, K.C., 2012, Tremor asperities in the transition zone control evolution of slow earthquakes: Journal of Geophysical Research. Solid Earth, v. 117, B10301, https://doi.org/10.1029/2012JB009249.

Grasemann, B., Schneider, D.A., Stockli, D.F., and Iglseder, C., 2012, Miocene bivergent crustal extension in the Aegean: Evidence from the western Cyclades (Greece): Lithosphere, v. 4, no. 1, p. 23–39, https://doi.org/10.1130/L164.1.

Gulick, S.P., Austin, J.A., McNeill, L.C., Bangs, N.L., Martin, K.M., Henstock, T.J., Bull, J.M., Dean, S., Djajadihardja, Y.S., and Permana, H., 2011, Updip rupture of the 2004 Sumatra earthquake extended by thick indurated sediments: Nature Geoscience, v. 4, no. 7, p. 453–456, https://doi.org/10.1038/ngeo1176.

Hacker, B.R., 1996, Eclogite formation and the rheology, buoyancy, seismicity, and H_2O content of oceanic crust, *in* Bebout, G.E., Scholl, D., and Kirby, S., eds., Subduction Top to Bottom: American Geophysical Union, Geophysical Monograph 96, p. 337–346, https://doi.org/10.1029/GM096p0337.

Handy, M.R., 1989, Deformation regimes and the rheological evolution of fault zones in the lithosphere: The effects of pressure, temperature, grainsize and time: Tectonophysics, v. 163, no. 1–2, p. 119–152, https://doi.org/10.1016/0040-1951(89)90122-4.

Handy, M.R., 1990, The solid-state flow of polymineralic rocks: Journal of Geophysical Research. Solid Earth, v. 95, no. B6, p. 8647–8661, https://doi.org/10.1029/JB095iB06p08647.

Handy, M.R., 1994, Flow laws for rocks containing two non-linear viscous phases: A phenomenological approach: Journal of Structural Geology, v. 16, no. 3, p. 287–301, https://doi.org/10.1016/0191-8141(94)90035-3.

Hayman, N.W., and Lavier, L.L., 2014, The geologic record of deep episodic tremor and slip: Geology, v. 42, no. 3, p. 195–198, https://doi.org/10.1130/G34990.1.

Hicks, S.P., Rietbrock, A., Haberland, C.A., Ryder, I.M.A., Simons, M., and Tassara, A., 2012, The 2010 Mw 8.8 Maule, Chile earthquake: Nucleation and rupture propagation controlled by a subducted topographic high: Geophysical Research Letters, v. 39, no. 19, https://doi.org/10.1029/2012GL053184.

Hilairet, N., Reynard, B., Wang, Y., Daniel, I., Merkel, S., Nishiyama, N., and Petitgirard, S., 2007, High-pressure creep of serpentine, interseismic deformation, and initiation of subduction: Science, v. 318, no. 5858, p. 1910–1913, https://doi.org/10.1126/science.1148494.

Hirth, G., and Kohlstedt, D.L., 2003, Rheology of the upper mantle and the mantle wedge: A view from the experimentalists: American Geophysical Union, Geophysical Monograph, v. 138, p. 83–105.

Hirth, G., Teyssier, C., and Dunlap, W.J., 2001, An evaluation of quartzite flow laws based on comparisons between experimentally and naturally deformed rocks: International Journal of Earth Sciences, v. 90, no. 1, p. 77–87, https://doi.org/10.1007/s005310000152.

Husen, S., Kissling, E., and Quintero, R., 2002: Tomographic evidence for a subducted seamount beneath the Gulf of Nicoya, Costa Rica: The cause of the 1990 Mw = 7.0 Gulf of Nicoya earthquake: Geophysical Research Letters, v. 29, p. 79-1–79-4.

Ide, S., Shelly, D.R., and Beroza, G.C., 2007, Mechanism of deep low frequency earthquakes: Further evidence that deep non-volcanic tremor is generated by shear slip on the plate interface: Geophysical Research Letters, v. 34, no. 3, https://doi.org/10.1029/2006GL028890.

Ito, Y., and Obara, K., 2006, Dynamic deformation of the accretionary prism excites very low frequency earthquakes: Geophysical Research Letters, v. 33, no. 2, https://doi.org/10.1029/2005GL025270.

Ito, Y., Obara, K., Shiomi, K., Sekine, S., and Hirose, H., 2007, Slow Earthquakes Coincident with Episodic Tremors and Slow Slip Events: Science, v. 315, p. 503–506, https://doi.org/10.1126/science.1134454.

Ito, Y., Hino, R., Kido, M., Fujimoto, H., Osada, Y., Inazu, D., Ohta, Y., Iinuma, T., Ohzono, M., Miura, S., Mishina, M., Suzuki, K., Tsuji, T., and Ashi, J., 2013, Episodic slow slip events in the Japan subduction zone before the 2011 Tohoku-Oki earthquake: Tectonophysics, v. 600, p. 14–26, https://doi.org/10.1016/j.tecto.2012.08.022.

Jansen, J.B.H., 1977, The geology of Naxos: Geological and Geophysical Studies, v. 19, p. 1–3.

Jessell, M.W., Bons, P.D., Griera, A., Evans, L.A., and Wilson, C.J., 2009, A tale of two viscosities: Journal of Structural Geology, v. 31, no. 7, p. 719–736, https://doi.org/10.1016/j.jsg.2009.04.010.

Ji, S., 2004, A generalized mixture rule for estimating the viscosity of solid-liquid suspensions and mechanical properties of polyphase rocks and composite materials: Journal of Geophysical Research. Solid Earth, v. 109, B10207, https://doi.org/10.1029/2004JB003124.

Jolivet, L., and Brun, J.P., 2010, Cenozoic geodynamic evolution of the Aegean: International Journal of Earth Sciences, v. 99, no. 1, p. 109–138, https://doi.org/10.1007/s00531-008-0366-4.

Jolivet, L., Faccenna, C., Goffé, B., Burov, E.B., and Agard, P., 2003, Subduction tectonics and exhumation of high-pressure metamorphic rocks in the Mediterranean orogens: American Journal of Science, v. 303, no. 5, p. 353–409, https://doi.org/10.2475/ajs.303.5.353.

Jolivet, L., Lecomte, E., Huet, B., Denèle, Y., Lacombe, O., Labrousse, L., Le Pourhiet, L., and Mehl, C., 2010a, The North Cycladic Detachment System: Earth and Planetary Science Letters, v. 289, p. 87–104, https://doi.org/10.1016/j.epsl.2009.10.032.

Jolivet, L., Trotet, F., Monie, P., Vidal, O., Goffé, B., Labrousse, L., Agard, P., and Ghorbal, B., 2010b, Along-strike variations of PT conditions in accretionary wedges and syn-orogenic extension, the HP-LT phyllite-quartzite nappe in Crete and the Peloponnese: Tectonophysics, v. 480, no. 1–4, p. 133–148, https://doi.org/10.1016/j.tecto.2009.10.002.

Jolivet, L., Faccenna, C., Huet, B., Labrousse, L., Le Pourhiet, L., Lacombe, O., Lecomte, E., Burov, E., Denèle, Y., Brun, J.P., Philippon, M., Paul, A., Salaün, G., Karabulut, H., Piromallo, C., Monié, P., Gueydan, F., Okay, A.I., Oberhänsli, R., Pourteau, A., Augier, R., Gadenne, L., and Driussi, O., 2013, Aegean tectonics: Strain localisation, slab tearing and trench retreat: Tectonophysics, v. 597–598, p. 1–33, https://doi.org/10.1016/j.tecto.2012.06.011.

Kameyama, M., Yuen, D.A., and Fujimoto, H., 1997, The interaction of viscous heating with grain-size dependent rheology in the formation of localized slip zones: Geophysical Research Letters, v. 24, no. 20, p. 2523–2526, https://doi.org/10.1029/97GL02648.

Kanamori, H., 1977, The energy release in great earthquakes: Journal of Geophysical Research, v. 82, no. 20, p. 2981–2987, https://doi.org/10.1029/JB082i020p02981.

Kanamori, H., 1986, Rupture process of subduction-zone earthquakes: Annual Review of Earth and Planetary Sciences, v. 14, no. 1, p. 293–322, https://doi.org/10.1146/annurev.ea.14.050186.001453.

Kao, H., Shan, S.-J., Dragert, H., Rogers, G., Cassidy, J.F., and Ramachandran, K., 2005, A wide depth distribution of seismic tremors along the northern Cascadia margin: Nature, v. 436, no. 7052, p. 841–844, https://doi.org/10.1038/nature03903.

Kao, H., Shan, S.J., Rogers, G., and Dragert, H., 2007, Migration characteristics of seismic tremors in the northern Cascadia margin: Geophysical Research Letters, v. 34, no. 3, https://doi.org/10.1029/2006GL028430.

Kao, H., Wang, K., Dragert, H., Kao, J.Y., and Rogers, G., 2010, Estimating seismic moment magnitude of tremor bursts in northern Cascadia: Implications for the "seismic efficiency" of episodic tremor and slip: Geophysical Research Letters, v. 37, L19306, https://doi.org/10.1029/2010GL044927.

Keiter, M., Piepjohn, K., Ballhaus, C., Lagos, M., and Bode, M., 2004, Structural development of high-pressure metamorphic rocks on Syros island (Cyclades, Greece): Journal of Structural Geology, v. 26, no. 8, p. 1433–1445, https://doi.org/10.1016/j.jsg.2003.11.027.

Keiter, M., Ballhaus, C., and Tomaschek, F., 2011, A new geological map of the Island of Syros (Aegean Sea, Greece): Implications for lithostratigraphy and structural history of the Cycladic Blueschist Unit: Geological Society of America Special Paper 481, p. 1–43, https://doi.org/10.1130/2011.2481.

Kenkmann, T., and Dresen, G., 2002, Dislocation microstructure and phase distribution in a lower crustal shear zone: International Journal of Earth Sciences, https://doi.org/10.1007/s00531-001-0236-9.
Kim, D., Katayama, I., Michibayashi, K., and Tsujimori, T., 2013, Rheological contrast between glaucophane and lawsonite in naturally deformed blueschist from Diablo Range, California: The Island Arc, v. 22, no. 1, p. 63–73, https://doi.org/10.1111/iar.12003.
Kimura, G., and Mukai, A., 1991, Underplated units in an accretionary complex: Melange of the Shimanto Belt of eastern Shikoku, southwest Japan: Tectonics, v. 10, no. 1, p. 31–50, https://doi.org/10.1029/90TC00799.
King, S.D., and Hager, B.H., 1990, The relationship between plate velocity and trench viscosity in Newtonian and power-law subduction calculations: Geophysical Research Letters, v. 17, no. 13, p. 2409–2412, https://doi.org/10.1029/GL017i013p02409.
Kirby, S.H., 1985, Rock mechanics observations pertinent to the rheology of the continental lithosphere and the localization of strain along shear zones: Tectonophysics, v. 119, no. 1–4, p. 1–27, https://doi.org/10.1016/0040-1951(85)90030-7.
Kronenberg, A.K., Kirby, S.H., and Pinkston, J., 1990, Basal slip and mechanical anisotropy of biotite: Journal of Geophysical Research. Solid Earth, v. 95, B12, p. 19,257–19,278, https://doi.org/10.1029/JB095iB12p19257.
Kurz, W., Neubauer, F., and Dachs, E., 1998, Eclogite meso- and microfabrics: Implications for the burial and exhumation history of eclogites in the Tauern Window (Eastern Alps) from P-T-d paths: Tectonophysics, v. 285, no. 1–2, p. 183–209, https://doi.org/10.1016/S0040-1951(97)00188-1.
Lagos, M., Scherer, E.E., Tomaschek, F., Munker, C., Keiter, M., Berndt, J., and Ballhaus, C., 2007, High precision Lu-Hf geochronology of Eocene eclogite-facies rocks from Syros, Cyclades, Greece: Chemical Geology, v. 243, no. 1, p. 16–35, https://doi.org/10.1016/j.chemgeo.2007.04.008.
Lardeaux, J., and Spalla, M., 1991, From granulites to eclogites in the Sesia zone (Italian Western Alps): A record of the opening and closure of the piedmont ocean: Journal of Metamorphic Geology, v. 9, no. 1, p. 35–59, https://doi.org/10.1111/j.1525-1314.1991.tb00503.x.
Laurent, V., Jolivet, L., Roche, V., Augier, R., Scaillet, S., and Cardello, G.L., 2016, Strain localization in a fossilized subduction channel: Insights from the Cycladic Blueschist Unit (Syros, Greece): Tectonophysics, v. 672, p. 150–169, https://doi.org/10.1016/j.tecto.2016.01.036.
Laurent, V., Lanari, P., Naïr, I., Augier, R., Lahfid, A., and Jolivet, L., 2018, Exhumation of eclogite and blueschist (Cyclades, Greece): Pressure-temperature evolution determined by thermobarometry and garnet equilibrium modelling: Journal of Metamorphic Geology, https://doi.org/10.1111/jmg.12309.
Li, H., Wei, M., Li, D., Liu, Y., Kim, Y.H., and Zhou, S., 2018, Segmentation of slow slip events in south central Alaska possibly controlled by a subducted oceanic plateau: Journal of Geophysical Research. Solid Earth, v. 123, no. 1, p. 418–436, https://doi.org/10.1002/2017JB014911.
Liu, Y., and Rice, Y., 2005, Aseismic slip transients emerge spontaneously in three-dimensional rate and state modeling of subduction earthquake sequences: Journal of Geophysical Research. Solid Earth, v. 110, B08307, https://doi.org/10.1029/2004JB003424.
Liu, Y., and Rice, J.R., 2007, Spontaneous and triggered aseismic deformation transients in a subduction fault model: Journal of Geophysical Research, v. 112, B09404, https://doi.org/10.1029/2007JB004930.
Lloyd, G.E., and Ferguson, C.C., 1981, Boudinage structure: Some new interpretations based on elastic-plastic finite element simulations: Journal of Structural Geology, v. 3, no. 2, p. 117–128, https://doi.org/10.1016/0191-8141(81)90009-2.
Malatesta, C., Federico, L., Crispini, L., and Capponi, G., 2018, Fluid-controlled deformation in blueschist-facies conditions: Plastic vs brittle behaviour in a brecciated mylonite (Voltri Massif, Western Alps, Italy): Geological Magazine, v. 155, no. 2, p. 335–355, https://doi.org/10.1017/S0016756816001163.
Masini, E., Manatschal, G., and Mohn, G., 2013, The Alpine Tethys rifted margins: Reconciling old and new ideas to understand the stratigraphic architecture of magma-poor rifted margins: Sedimentology, v. 60, no. 1, p. 174–196, https://doi.org/10.1111/sed.12017.
McCaffrey, R., Wallace, L.M., and Beavan, J., 2008, Slow slip and frictional transition at low temperature at the Hikurangi subduction zone: Nature Geoscience, v. 1, no. 5, p. 316–320, https://doi.org/10.1038/ngeo178.
Meneghini, F., and Moore, J.C., 2007, Deformation and hydrofracture in a subduction thrust at seismogenic depths: The Rodeo Cove thrust zone, Marin Headlands, California: Geological Society of America Bulletin, v. 119, no. 1–2, p. 174–183, https://doi.org/10.1130/B25807.1.
Moore, J.C., 1995, Abnormal fluid pressures and fault-zone dilation in the Barbados accretionary prism: Evidence from logging while drilling: Geology, v. 23, no. 7, p. 605–608, https://doi.org/10.1130/0091-7613(1995)023<0605:AFPAFZ>2.3.CO;2.
Moore, J.C., and Saffer, D., 2001, Updip limit of the seismogenic zone beneath the accretionary prism of southwest Japan: An effect of diagenetic to low-grade metamorphic processes and increasing effective stress: Geology, v. 29, no. 2, p. 183–186, https://doi.org/10.1130/0091-7613(2001)029<0183:ULOTSZ>2.0.CO;2.
Norris, R.J., and Cooper, A.F., 2003, Very high strains recorded in mylonites along the Alpine Fault, New Zealand: Implications for the deep structure of plate boundary faults: Journal of Structural Geology, v. 25, no. 12, p. 2141–2157, https://doi.org/10.1016/S0191-8141(03)00045-2.
Obara, K., 2002, Nonvolcanic deep tremor associated with subduction in southwest Japan: Science, v. 296, no. 5573, p. 1679–1681, https://doi.org/10.1126/science.1070378.
Obara, K., and Hirose, H., 2006, Non-volcanic deep low-frequency tremors accompanying slow slips in the southwest Japan subduction zone: Tectonophysics, v. 417, no. 1–2, p. 33–51, https://doi.org/10.1016/j.tecto.2005.04.013.
Okrusch, M., and Bröcker, M., 1990, Eclogites associated with high-grade blueschists in the Cyclades archipelago, Greece: A review: European Journal of Mineralogy, v. 2, no. 4, p. 451–478, https://doi.org/10.1127/ejm/2/4/0451.
Oleskevich, D.A., Hyndman, R.D., and Wang, K., 1999, The updip and downdip limits to great subduction earthquakes: Thermal and structural models of Cascadia, south Alaska, SW Japan, and Chile: Journal of Geophysical Research. Solid Earth, v. 104, p. 14965–14991, https://doi.org/10.1029/1999JB900060.
Papanikolaou, D., 2013, Tectonostratigraphic models of the Alpine terranes and subduction history of the Hellenides: Tectonophysics, v. 595–596, p. 1–24, https://doi.org/10.1016/j.tecto.2012.08.008.
Péron-Pinvidic, G., Manatschal, G., Minshull, T.A., and Sawyer, D.S., 2007, Tectonosedimentary evolution of the deep Iberia-Newfoundland margins: Evidence for a complex breakup history: Tectonics, v. 26, TC2011, https://doi.org/10.1029/2006TC001970.
Peterson, C.L., and Christensen, D.H., 2009, Possible relationship between nonvolcanic tremor and the 1998–2001 slow slip event, south central Alaska: Journal of Geophysical Research. Solid Earth, v. 114, B06302, https://doi.org/10.1029/2008JB006096.
Philippon, M., Brun, J.P., and Gueydan, F., 2011, Tectonics of the Syros blueschists (Cyclades, Greece): From subduction to Aegean extension: Tectonics, v. 30, https://doi.org/10.1029/2010TC002810.
Philippon, M., Brun, J.P., and Gueydan, F., 2012, Deciphering subduction from exhumation in the segmented Cycladic Blueschist Unit (Central Aegean, Greece): Tectonophysics, https://doi.org/10.1016/j.tecto.2011.12.025.
Philippon, M., Gueydan, F., Pitra, P., and Brun, J.P., 2013, Preservation of subduction-related prograde deformation in lawsonite pseudomorph-bearing rocks: Journal of Metamorphic Geology, v. 31, no. 5, p. 571–583, https://doi.org/10.1111/jmg.12035.
Plank, T., and Langmuir, C.H., 1993, Tracing trace elements from sediment input to volcanic output at subduction zones: Nature, v. 362, no. 6422, p. 739, https://doi.org/10.1038/362739a0.
Platt, J.P., Xia, H., and Schmidt, W.L., 2018, Rheology and stress in subduction zones around the aseismic/seismic transition: Progress in Earth and Planetary Science, v. 5, p. 1–12, https://doi.org/10.1186/s40645-018-0183-8.
Poirier, J.P., 1985, Creep of Crystals: High-temperature Deformation Processes in Metals, Ceramics and Minerals: Cambridge University Press, Online ISBN: 9780511564451, https://doi.org/10.1017/CBO9780511564451.
Putlitz, B., Matthews, A., and Valley, J.W., 2000, Oxygen and hydrogen isotope study of high-pressure metagabbros and metabasalts (Cyclades, Greece): Implications for the subduction of oceanic crust: Contributions to Mineralogy and Petrology, v. 138, p. 114–126, https://doi.org/10.1007/s004100050012.
Putlitz, B., Cosca, M.A., and Schumacher, J.C., 2005, Prograde mica $^{40}Ar/^{39}Ar$ growth ages recorded in high pressure rocks (Syros, Cyclades, Greece): Chemical Geology, v. 214, no. 1–2, p. 79–98, https://doi.org/10.1016/j.chemgeo.2004.08.056.
Rawling, T.J., and Lister, G.S., 2002, Large-scale structure of the eclogite-blueschist belt of New Caledonia: Journal of Structural Geology, v. 24, no. 8, p. 1239–1258, https://doi.org/10.1016/S0191-8141(01)00128-6.
Ridley, J., 1982, Arcuate lineation trends in a deep level, ductile thrust belt, Syros, Greece: Tectonophysics, v. 88, no. 3–4, p. 347–360, https://doi.org/10.1016/0040-1951(82)90246-3.
Ring, U., and Glodny, J., 2010, No need for lithospheric extension for exhuming (U)HP rocks by normal faulting: Journal of the Geological Society of London, v. 167, no. 2, p. 225, https://doi.org/10.1144/0016-76492009-134.
Ring, U., Layer, P.W., and Reischmann, T., 2001, Miocene high-pressure metamorphism in the Cyclades and Crete, Aegean Sea, Greece: Evidence for large-magnitude displacement on

the Cretan detachment: Geology, v. 29, no. 5, p. 395–398, https://doi.org/10.1130/0091-7613(2001)029<0395:MHPMIT>2.0.CO;2.
Ring, U., Thomson, S.N., and Bröcker, M., 2003, Fast extension but little exhumation: The Vari detachment in the Cyclades, Greece: Geological Magazine, v. 140, no. 3, p. 245–252, https://doi.org/10.1017/S0016756803007799.
Ring, U., Glodny, J., Will, T., and Thomson, S., 2010, The Hellenic subduction system: high-pressure metamorphism, exhumation, normal faulting, and large-scale extension: Annual Review of Earth and Planetary Sciences, v. 38, p. 45–76, https://doi.org/10.1146/annurev.earth.050708.170910.
Rogers, G., and Dragert, H., 2003, Episodic tremor and slip on the Cascadia subduction zone: The chatter of silent slip: Science, v. 300, no. 5627, p. 1942–1943, https://doi.org/10.1126/science.1084783.
Rosenbaum, G., Avigad, D., and Sánchez-Gómez, M., 2002, Coaxial flattening at deep levels of orogenic belts: Evidence from blueschists and eclogites on Syros and Sifnos (Cyclades, Greece): Journal of Structural Geology, v. 24, p. 1451–1462, https://doi.org/10.1016/S0191-8141(01)00143-2.
Royden, L.H., 1993, The tectonic expression of slab pull at continental convergent boundaries: Tectonics, v. 12, no. 2, p. 303–325, https://doi.org/10.1029/92TC02248.
Rubie, D.C., 1983, Reaction-enhanced ductility: The role of solid-solid univariant reactions in deformation of the crust and mantle: Tectonophysics, v. 96, no. 3–4, p. 331–352, https://doi.org/10.1016/0040-1951(83)90225-1.
Rubin, A.M., 2008, Episodic slow slip events and rate-and-state friction: Journal of Geophysical Research. Solid Earth, v. 113, p. B11,414–B11,418, https://doi.org/10.1029/2008JB005642.
Rubinstein, J.L., La Rocca, M., Vidale, J.E., Creager, K.C., and Wech, A.G., 2008, Tidal modulation of nonvolcanic tremor: Science, v. 319, no. 5860, p. 186–189, https://doi.org/10.1126/science.1150558.
Saffer, D.M., and Wallace, L.M., 2015, The frictional, hydrologic, metamorphic and thermal habitat of shallow slow earthquakes: Nature Geoscience, v. 8, no. 8, p. 594–600, https://doi.org/10.1038/ngeo2490.
Schliestedt, M., 1986, Eclogite-blueschist relationships as evidenced by mineral equilibria in the high-pressure metabasic rocks of Sifnos (Cycladic Islands), Greece: Journal of Petrology, v. 27, no. 6, p. 1437–1459, https://doi.org/10.1093/petrology/27.6.1437.
Schmädicke, E., and Will, T.M., 2003, Pressure-temperature evolution of blueschist facies rocks from Sifnos, Greece, and implications for the exhumation of high-pressure rocks in the Central Aegean: Journal of Metamorphic Geology, v. 21, p. 799–811, https://doi.org/10.1046/j.1525-1314.2003.00482.x.
Schmalholz, S.M., and Maeder, X., 2012, Pinch-and-swell structure and shear zones in viscoplastic layers: Journal of Structural Geology, v. 37, p. 75–88, https://doi.org/10.1016/j.jsg.2012.01.026.
Schmid, S.M., Paterson, M.S., and Boland, J.N., 1980, High temperature flow and dynamic recrystallization in Carrara marble: Tectonophysics, v. 65, no. 3–4, p. 245–280, https://doi.org/10.1016/0040-1951(80)90077-3.
Schmidt, D.A., and Gao, H., 2010, Source parameters and time-dependent slip distributions of slow slip events on the Cascadia subduction zone from 1998 to 2008: Journal of Geophysical Research. Solid Earth, v. 115, no. 4.
Schneider, D.A., Grasemann, B., Lion, A., Soukis, K., and Draganits, E., 2018, Geodynamic significance of the Santorini detachment system (Cyclades, Greece): Terra Nova.
Schramm, B., Devey, C.W., Gillis, K.M., and Lackschewitz, K., 2005, Quantitative assessment of chemical and mineralogical changes due to progressive low-temperature alteration of East Pacific Rise basalts from 0 to 9 Ma: Chemical Geology, v. 218, no. 3–4, p. 281–313, https://doi.org/10.1016/j.chemgeo.2005.01.011.
Schumacher, J.C., Brady, J.B., Cheney, J.T., and Tonnsen, R.R., 2008, Glaucophane-bearing marbles on Syros, Greece: Journal of Petrology, v. 49, p. 1667–1686, https://doi.org/10.1093/petrology/egn042.
Seck, H.A., Koetz, J., Okrusch, M., Seidel, E., and Stosch, H.-G., 1996, Geochemistry of a meta-ophiolite suite: An associated metagabbros, eclogites and glaucophanites on the island of Syros, Greece: European Journal of Mineralogy, v. 8, no. 3, p. 607–624, https://doi.org/10.1127/ejm/8/3/0607.
Segall, P., and Bradley, A.M., 2012, Slow-slip evolves into megathrust earthquakes in 2D numerical simulations: Geophysical Research Letters, v. 39, no. 17.
Sheldon, H., and Ord, A., 2005, Evolution of porosity, permeability and fluid pressure in dilatant faults post-failure: Implications for fluid flow and mineralization: Geofluids, v. 5, no. 4, p. 272–288, https://doi.org/10.1111/j.1468-8123.2005.00120.x.
Sheldon, H.A., and Micklethwaite, S., 2007, Damage and permeability around faults: Implications for mineralization: Geology, v. 35, no. 10, p. 903–906, https://doi.org/10.1130/G23860A.1.
Shelly, D.R., and Hardebeck, J.L., 2010, Precise tremor source locations and amplitude variations along the lower-crustal central San Andreas Fault: Geophysical Research Letters, v. 37, no. 14, https://doi.org/10.1029/2010GL043672.
Shelly, D.R., Beroza, G.C., Ide, S., and Nakamula, S., 2006, Low-frequency earthquakes in Shikoku, Japan, and their relationship to episodic tremor and slip: Nature, v. 442, no. 7099, p. 188–191, https://doi.org/10.1038/nature04931.
Shelly, D.R., Beroza, G.C., and Ide, S., 2007a, Complex evolution of transient slip derived from precise tremor locations in western Shikoku, Japan: Geochemistry Geophysics Geosystems, v. 8, no. 10, https://doi.org/10.1029/2007GC001640.
Shelly, D.R., Beroza, G.C., and Ide, S., 2007b, Non-volcanic tremor and low-frequency earthquake swarms: Nature, v. 446, p. 305–307, https://doi.org/10.1038/nature05666.
Shibazaki, B., 2003, On the physical mechanism of silent slip events along the deeper part of the seismogenic zone: Geophysical Research Letters, v. 30, no. 9, p. 1489, https://doi.org/10.1029/2003GL017047.
Shibazaki, B., and Shimamoto, T., 2007, Modelling of short-interval silent slip events in deeper subduction interfaces considering the frictional properties at the unstable-stable transition regime: Geophysical Journal International, v. 171, no. 1, p. 191–205, https://doi.org/10.1111/j.1365-246X.2007.03434.x.
Shimamoto, T., 1986, Transition between frictional slip and ductile flow for halite shear zones at room temperature: Science, v. 231, no. 4739, p. 711–714, https://doi.org/10.1126/science.231.4739.711.
Skarbek, R.M., and Rempel, A.W., 2016, Dehydration-induced porosity waves and episodic tremor and slip: Geochemistry, Geophysics, Geosystems, v. 17, no. 2, p. 442–469, https://doi.org/10.1002/2015GC006155.
Skelton, A., Peillod, A., Glodny, J., Klonowska, I., Månbro, C., Lodin, K., and Ring, U., 2018, Preservation of high-*P* rocks coupled to rock composition and the absence of metamorphic fluids: Journal of Metamorphic Geology, https://doi.org/10.1111/jmg.12466.
Skemer, P., Katayama, I., Jiang, Z., and Karato, S.I., 2005, The misorientation index: Development of a new method for calculating the strength of lattice-preferred orientation: Tectonophysics, v. 411, p. 157–167, https://doi.org/10.1016/j.tecto.2005.08.023.
Soukis, K., and Stockli, D.F., 2013, Structural and thermochronometric evidence for multi-stage exhumation of southern Syros, Cycladic islands, Greece: Tectonophysics, v. 595–596, p. 148–164, https://doi.org/10.1016/j.tecto.2012.05.017.
Spandler, C., Hermann, J., Arculus, R., and Mavrogenes, J., 2004, Geochemical heterogeneity and element mobility in deeply subducted oceanic crust: Insights from high-pressure mafic rocks from New Caledonia: Chemical Geology, v. 206, p. 21–42, https://doi.org/10.1016/j.chemgeo.2004.01.006.
Stern, C.R., 2011, Subduction erosion: Rates, mechanisms, and its role in arc magmatism and the evolution of the continental crust and mantle: Gondwana Research, v. 20, no. 2–3, p. 284–308, https://doi.org/10.1016/j.gr.2011.03.006.
Stöckhert, B., 2002, Stress and deformation in subduction zones: Insight from the record of exhumed metamorphic rocks, *in* De Meer, S., Drury, M.R., De Bresser, J.H.P., and Pennock, G.M., eds., Deformation Mechanisms, Rheology and Tectonics: Current Status and Future Perspectives: Geological Society of London Special Publication 200, p. 255, https://doi.org/10.1144/GSL.SP.2001.200.01.15.
Stöckhert, B., Wachmann, M., Küster, M., and Bimmermann, S., 1999, Low effective viscosity during high pressure metamorphism due to dissolution precipitation creep: The record of HP-LT metamorphic carbonates and siliciclastic rocks from Crete: Tectonophysics, v. 303, no. 1–4, p. 299–319, https://doi.org/10.1016/S0040-1951(98)00262-5.
Sweet, J.R., Creager, K.C., and Houston, H., 2014, A family of repeating low-frequency earthquakes at the downdip edge of tremor and slip: Geochemistry, Geophysics, Geosystems, v. 15, no. 9, p. 3713–3721, https://doi.org/10.1002/2014GC005449.
Szeliga, W., Melbourne, T., Santillan, M., and Miller, M., 2008, GPS constraints on 34 slow slip events within the Cascadia subduction zone, 1997–2005: Journal of Geophysical Research. Solid Earth, v. 113, no. 4.
Tera, F., Brown, L., Morris, J., Sacks, I.S., Klein, J., and Middleton, R., 1986, Sediment incorporation in island-arc magmas: Inferences from ^{10}Be: Geochimica et Cosmochimica Acta, v. 50, no. 4, p. 535–550, https://doi.org/10.1016/0016-7037(86)90103-1.
Thomas, A.M., Beroza, G.C., and Shelly, D.R., 2016, Constraints on the source parameters of low-frequency earthquakes on the San Andreas Fault: Geophysical Research Letters, v. 43, no. 4, p. 1464–1471, https://doi.org/10.1002/2015GL067173.

Tomaschek, F., Kennedy, A.K., Villa, I.M., Lagos, M., and Ballhaus, C., 2003, Zircons from Syros, Cyclades, Greece—Recrystallization and mobilization of zircon during high-pressure metamorphism: Journal of Petrology, v. 44, no. 11, p. 1977–2002, https://doi.org/10.1093/petrology/egg067.

Tomaschek, F., Keiter, M., Kennedy, A.K., and Ballhaus, C., 2008, Pre-alpine basement within the northern Cycladic Blueschist Unit on Syros Island, Greece: Zeitschrift der Deutschen Gesellschaft für Geowissenschaften, v. 159, p. 521–531, https://doi.org/10.1127/1860-1804/2008/0159-0521.

Trotet, F., Jolivet, L., and Vidal, O., 2001, Tectono-metamorphic evolution of Syros and Sifnos islands (Cyclades, Greece): Tectonophysics, v. 338, no. 2, p. 179–206, https://doi.org/10.1016/S0040-1951(01)00138-X.

von Huene, R., and Scholl, D.W., 1991, Observations at convergent margins concerning sediment subduction, subduction erosion, and the growth of continental crust: Reviews of Geophysics, v. 29, no. 3, p. 279–316, https://doi.org/10.1029/91RG00969.

Wallace, L.M., and Beavan, J., 2010, Diverse slow slip behavior at the Hikurangi subduction margin, New Zealand: Journal of Geophysical Research. Solid Earth, v. 115, B12402, https://doi.org/10.1029/2010JB007717.

Wallace, L.M., Beavan, J., Bannister, S., and Williams, C., 2012, Simultaneous long-term and short-term slow slip events at the Hikurangi subduction margin, New Zealand: Implications for processes that control slow slip event occurrence, duration, and migration: Journal of Geophysical Research. Solid Earth, v. 117, no. 11.

Wallace, L.M., Webb, S.C., Ito, Y., Mochizuki, K., Hino, R., Henrys, S., Schwartz, S.Y., and Sheehan, A.F., 2016, Slow slip near the trench at the Hikurangi subduction zone, New Zealand: Science, v. 352, no. 6286, p. 701–704, https://doi.org/10.1126/science.aaf2349.

Wang, Z., Zhao, D., Mishra, O.P., and Yamada, A., 2006, Structural heterogeneity and its implications for the low frequency tremors in Southwest Japan: Earth and Planetary Science Letters, v. 251, no. 1–2, p. 66–78, https://doi.org/10.1016/j.epsl.2006.08.025.

Wassmann, S., and Stöckhert, B., 2013, Rheology of the plate interface—Dissolution precipitation creep in high pressure metamorphic rocks: Tectonophysics, https://doi.org/10.1016/j.tecto.2013.09.030.

Watanabe, T., Hiramatsu, Y., and Obara, K., 2007, Scaling relationship between the duration and the amplitude of non-volcanic deep low-frequency tremors: Geophysical Research Letters, v. 34, no. 7, https://doi.org/10.1029/2007GL029391.

Webber, S., Ellis, S., and Fagereng, Å., 2018, "Virtual shear box" experiments of stress and slip cycling within a subduction interface mélange: Earth and Planetary Science Letters, v. 488, p. 27–35, https://doi.org/10.1016/j.epsl.2018.01.035.

White, W.M., and Dupré, B., 1986, Sediment subduction and magma genesis in the Lesser Antilles: Isotopic and trace element constraints: Journal of Geophysical Research, v. 91, B6, p. 5927, https://doi.org/10.1029/JB091iB06p05927.

Xia, H., and Platt, J.P., 2017, Structural and rheological evolution of the Laramide subduction channel in southern California: Solid Earth, v. 8, no. 2, https://doi.org/10.5194/se-8-379-2017.

Zhang, J., and Green, H.W., 2007, Experimental investigation of eclogite rheology and its fabrics at high temperature and pressure: Journal of Metamorphic Geology, v. 25, no. 2, p. 97–115, https://doi.org/10.1111/j.1525-1314.2006.00684.x.

Zhang, J., Green, H.W., II, and Bozhilov, K.N., 2006, Rheology of omphacite at high temperature and pressure and significance of its lattice preferred orientations: Earth and Planetary Science Letters, v. 246, no. 3–4, p. 432–443, https://doi.org/10.1016/j.epsl.2006.04.006.